PACIFIC EARTHQUAKE ENGINEERING
RESEARCH CENTER

NGA-West2 Models for Ground-Motion Directionality

Shrey K. Shahi
Jack W. Baker

Department of Civil and Environmental Engineering
Stanford University

PEER 2013/10
MAY 2013

Disclaimer

The opinions, findings, and conclusions or recommendations expressed in this publication are those of the author(s) and do not necessarily reflect the views of the study sponsor(s) or the Pacific Earthquake Engineering Research Center.

NGA-West2 Models for Ground-Motion Directionality

Shrey K. Shahi

Jack W. Baker

Department of Civil and Environmental Engineering
Stanford University

PEER Report 2013/10
Pacific Earthquake Engineering Research Center
Headquarters, University of California, Berkeley

May 2013

ABSTRACT

The NGA-West2 research program, coordinated by the Pacific Earthquake Engineering Research Center (PEER), is a major effort to produce refined models for predicting ground-motion response spectra. This study presents new models for ground-motion directionality developed as part of that project. Using a database of recorded strong ground motions, empirical models have been developed for a variety of quantities related to direction-dependent spectra. Predictions are available for the maximum spectral acceleration observed in any orientation of two-component horizontal ground-motion shaking ($Sa_{RotD100}$). This model is formulated as a multiplier factor to be coupled with the NGA-West2 models that predict the median spectral accelerations over all orientations (Sa_{RotD50}). Models are also proposed for the distribution of orientations of the $Sa_{RotD100}$ value relative to the fault and the relationship between $Sa_{RotD100}$ orientation at different periods. Discussion is provided as to how these results can be applied to practical seismic hazard analysis and compute realistic target spectra conditioned on different parameters.

ACKNOWLEDGMENTS

This study was sponsored by the Pacific Earthquake Engineering Research Center (PEER) and funded by the California Earthquake Authority, California Department of Transportation, and the Pacific Gas & Electric Company. Any opinions, findings, and conclusions or recommendations expressed in this material are those of the authors and do not necessarily reflect those of the above-mentioned agencies We thank the NGA West 2 Directionality Working group, consisting of Brian Chiou, Nico Luco, Mahmoud Hachem, Badie Rowshandel Tom Shantz Paul Spudich, and Jonathan Stewart for their helpful feedback and suggestions for this work. We also thank Yousef Bozorgnia and Carola Di Alessandro for their feedback and guidance, and Silvia Mazzoni for review comments.

CONTENTS

LIST OF FIGURES

LIST OF TABLES

1 INTRODUCTION

Structures designed to resist seismic loads are generally designed considering ground motion in the horizontal plane. However, the acceleration response spectrum, which is the intensity-measure (IM) used for design, is defined as the maximum response of a damped single-degree-of-freedom (SDOF) system at different periods when excited by a single component of the ground motion (5% damping is assumed throughout, also Sa in this report refers to pseudo spectral acceleration or PSA). So, even though two dimensional ground motions are considered for design, the IM is defined to represent single component of the ground motion. Various methods have been proposed to compute an intensity-measure representative of the two-dimensional horizontal ground motion. These methods include using the geometric mean of the acceleration response spectra computed using two orthogonal components of ground motion, using the median or maximum value of response spectra over all orientations at each period, etc. [Boore et al. 2006; Boore 2010].

The NGA-West2 research program, coordinated by Pacific Earthquake Engineering Research Center (PEER), produces refined models for predicting the median ground-motion response spectra of a ground motion when rotated over all horizontal orientations (Bozorgnia et al. 2012); this is referred to as the Sa_{RotD50} spectrum [Boore 2010]. It is known that ground-motion intensity is not uniform in all orientations. In some cases ground motions can be polarized and intensity in one orientation can be significantly stronger than in other orientations (e.g., Campbell and Bozorgnia [2007, 2008]; and Huang et al. [2008]). This phenomenon is often referred as "directionality" of ground motion. Due to ground motion directionality, some engineers believe that the maximum spectral acceleration over all orientations ($Sa_{RotD100}$) is a more meaningful IM than Sa_{RotD50} for structural design (e.g., NEHRP [2009]). Thus, different definitions of ground-motion intensities will be used to build ground-motion models (Sa_{RotD50}) and for structural design ($Sa_{RotD100}$). The need to use a consistent IM throughout the design process (e.g., Baker and Cornell [2006]; and Beyer and Bommer [2006]) requires models to convert between the two definitions of IM. Additionally, there is interest in whether the $Sa_{RotD100}$ is observed in random orientations or has preferential alignment in, for example, near-fault ground motions. This also has potentially important implications for structural design.

Several researchers have modeled the ratio of different IMs, which can be used as a multiplicative factor to convert between them (e.g., Beyer and Bommer [2006]; Watson-Lamprey and Boore [2007]; Campbell and Bozorgnia [2007, 2008]; and Huang et al. [2008, 2010]). Most of these studies used subsets of the NGA database [Chiou et al. 2008] and focused on the ratios involving the older $Sa_{GMRotI50}$ definition of response spectrum. This study used over 3000 ground motions from the expanded NGA-West2 database to build empirical models for the ratio of $Sa_{RotD100}$ to Sa_{RotD50} and the probability distribution of orientations in which the

$Sa_{RotD100}$ is observed. The model predicting the ratio of $Sa_{RotD100}$ to Sa_{RotD50} can be used as a multiplicative factor that when used with the NGA-West2 ground-motion models can predict the $Sa_{RotD100}$ at a site. The proposed models are compared with older models and differences are discussed.

As defined, the $Sa_{RotD100}$ values at different periods may occur in differing orientations. So it is highly unlikely that any single orientation will have *Sa* as large as the $Sa_{RotD100}$ at all periods. Since nonlinear response of a multi-degree-of-freedom (MDOF) system is related to *Sa* at a range of periods, using $Sa_{RotD100}$ as the spectrum of a single ground-motion component may lead to conservative estimates of structural demand (e.g., Stewart et al. [2011]). To address this, the relationship between the orientations of $Sa_{RotD100}$ at different periods is studied in detail, and this information is used to compute more realistic target spectra for single ground-motion components. Example computation and discussion of several alternate target spectra is included.

2 Ground-Motion Intensity and Directionality

As discussed above, spectral acceleration (*Sa*) measures the response of a SDOF oscillator in a single orientation and cannot completely represent the intensity in two dimensions if the ground motion is polarized. Several IMs have been proposed in the past to better account for two dimensional intensity of ground motions, while not sacrificing the ease of use of a scalar IM. Early efforts to account for the two-dimensional intensity of ground motion used the geometric mean of response spectra computed using two orthogonal components of the ground motion (sometimes referred as Sa_{GM}). Generally the two orientations in which the ground motion was recorded ("as-recorded orientations"), or the fault-normal and parallel orientations, are used for computing Sa_{GM}. Using the as-recorded orientations of the ground motion makes the ground-motion intensity dependent on the orientation of the recording instrument, which is often arbitrary (though the practical effect on *Sa* is often not major). The fault-normal and parallel orientations are important for near-fault sites, as near-fault effects are generally observed in these orientations (directivity in fault-normal, fling in fault-parallel for strike-slip earthquakes), but these orientations have no special significance for sites located far from the fault.

To remove the dependence of IM on arbitrarily selected orientations, Boore et al. (2006) introduced $Sa_{GMRotDnn}$ and $Sa_{GMRotInn}$ IMs, which are orientation independent definitions of ground-motion intensity. $Sa_{GMRotDnn}$ is defined as the nn^{th} percentile of the geometric means of the response spectra from all orthogonal components of the ground motion at a specified period. The $Sa_{GMRotDnn}$ spectrum uses the geometric means from different orientations at different periods and does not represent any particular observation of two components of the ground motion. $Sa_{GMRotInn}$ addresses this problem by defining the intensity measure as the geometric mean of response spectra at the specific orientation with a spectrum closest to the $Sa_{GMRotDnn}$ spectrum across a range of periods. This definition uses the geometric mean spectrum of two specific ground-motion components that were observed at the site. The 2008 version of NGA ground-motion models were developed to predict the $Sa_{GMRotI50}$ at a site [Abrahamson et al. 2008].

Although the $Sa_{GMRotInn}$ spectrum captures information from multiple orientations and is orientation and period independent, it is difficult to compute. Boore [2010] proposed a new set of IM called Sa_{RotDnn} and Sa_{RotInn}. Sa_{RotDnn} is defined as the nn^{th} percentile of the spectral acceleration at each period over all orientations. Like $Sa_{GMRotDnn}$, the nn^{th} percentile spectral acceleration at each period may occur in different orientations. Sa_{RotInn} addresses this by defining the intensity to be the spectral acceleration in the orientation most representative of the Sa_{RotDnn} spectrum. Since maximum intensity at each period may occur in different orientations and Sa_{RotInn} spectrum uses a single orientation of the ground motion, the Sa_{RotI50} spectrum can be greater than the $Sa_{RotI100}$ spectrum at some periods [Boore 2010]. This is considered a shortcoming of the Sa_{RotInn} definition. Due to its simple and orientation-independent definition the Sa_{RotDnn} IM has become popular. The new ground-motion models being developed as part of the NGA-West2 project will predict Sa_{RotD50} values, but the NEHRP [2009] provisions use $Sa_{RotD100}$ intensity for seismic design.

In general, constructing a single response spectrum to represent two-dimensional ground-motion intensity involves reducing information in two dimensions to one, which results in loss of some information. Different definitions of ground-motion intensity capture different pieces of this information and thus may be appropriate for different tasks. If the ground motion is unpolarized, then it will have equal intensity in all orientations (i.e., no directionality). In an almost no-polarization case, illustrated in Figure 2.1a, all definitions of ground-motion intensity will give similar result. Hence, the ratio of $Sa_{RotD100}$ to Sa_{RotD50} will be close to 1. However, if the ground motion is strongly polarized, as illustrated in Figure 2.1b, the various definitions of Sa will differ significantly in value. In this case, different definitions of IM will give different results, and the ratio of $Sa_{RotD100}$ to Sa_{RotD50} can be shown to equal $\sqrt{2} = 1.414$. A ground-motion record generally lies between these two extreme cases, and the $Sa_{RotD100}$ to Sa_{RotD50} ratio lies between 1 and 1.414, as shown in Figure 2.2. So the intensity of ground motion computed using Sa_{RotD50} or $Sa_{RotD100}$ can differ for various ground motions, with the difference ranging from 0 to 41% of the Sa_{RotD50} intensity.

The polarization of ground motion, also referred as directionality of ground motion, causes this discrepancy among different definitions of response spectra. Thus, in this study the models used to convert between different spectral acceleration definitions are referred to as directionality models.

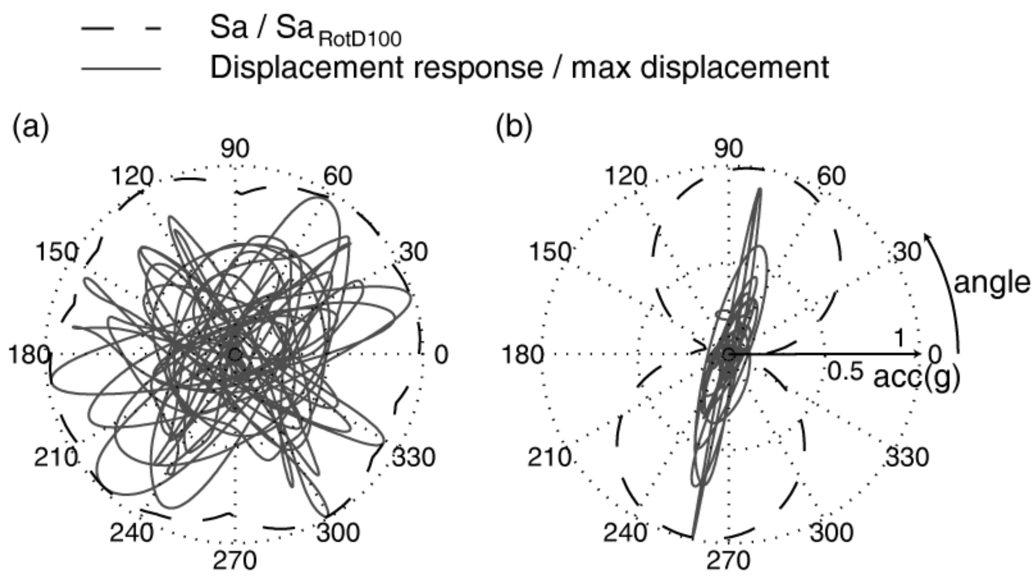

Figure 2.1 **Displacement response trace (*T* = 1 sec) and spectral acceleration in all orientations: (a) when ground motion is almost unpolarized (HWA031 recording from Chi-Chi-04, 1999 earthquake); and (b) when the ground motion is almost completely polarized (Gilroy Array#6 recording from Morgan Hill,1984 earthquake).**

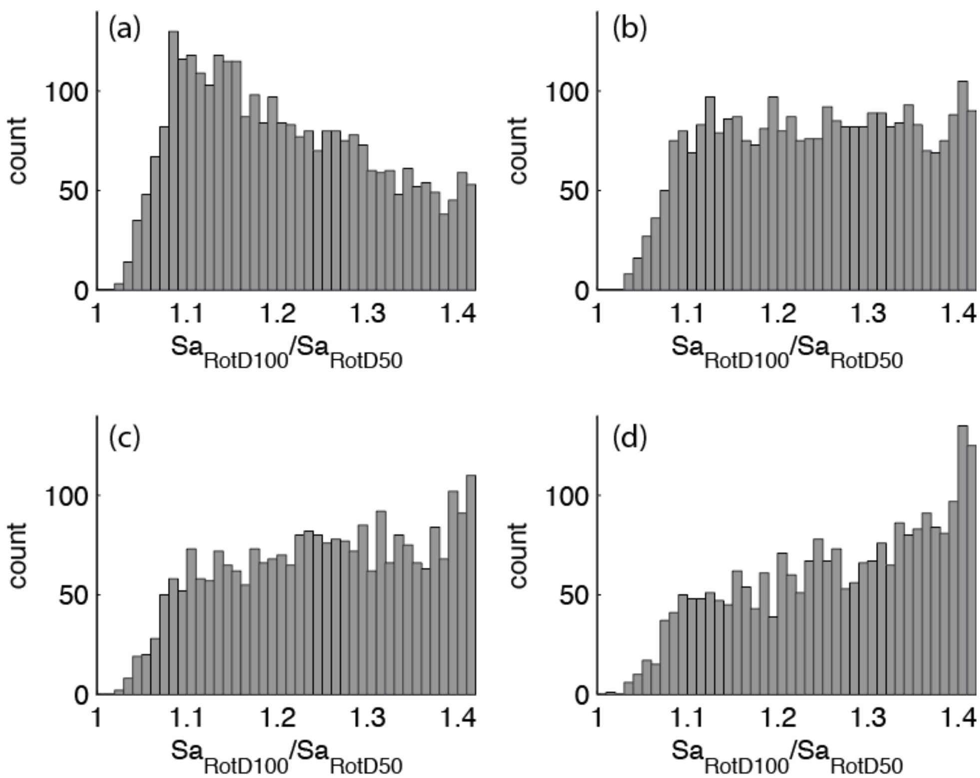

Figure 2.2 Histogram of observed ratios of $Sa_{RotD100}$ and Sa_{RotD50} in the NGA-West2 database for (a) *T* = 0.2 sec, (b) *T* = 1 sec, (c) *T* = 3 sec, and (d) *T* = 5 sec.

3 Ratio of $Sa_{RotD100}$ to Sa_{RotD50}

As discussed earlier, the NEHRP (2009) provisions use $Sa_{RotD100}$ as the IM for design while the NGA-West2 ground-motion models are being developed to predict Sa_{RotD50} intensity. Thus, models to convert between the two definitions are needed to allow the use of consistent definition of IM throughout the design process.

We computed the ratio of $Sa_{RotD100}$ to Sa_{RotD50} for each ground motion in the subset of NGA-West2 database being used to develop the Abrahamson-Silva ground-motion model. The geometric mean of these ratios can be used as a multiplicative factor to convert Sa_{RotD50} intensity to $Sa_{RotD100}$ and its logarithm as an additive factor to convert $lnSa_{RotD50}$ to $\ln Sa_{RotD100}$. As ground-motion intensities are assumed to be log-normally distributed (e.g., Abrahamson [1998]; and Jayaram and Baker [2008]) and the ground-motion models predict the natural log of intensity, the geometric mean of the ratios is a more natural estimator than the arithmetic mean, as shown in Equations (3.1) to (3.3).

$$Sa_{RotD100} = \frac{Sa_{RotD100}}{Sa_{RotD50}} \cdot Sa_{RotD50} \tag{3.1}$$

$$lnSa_{RotD100} = ln\left(\frac{Sa_{RotD100}}{Sa_{RotD50}}\right) + lnSa_{RotD50} \tag{3.2}$$

$$E[lnSa_{RotD100}] = E\left[ln\left(\frac{Sa_{RotD100}}{Sa_{RotD50}}\right)\right] + E[lnSa_{RotD50}] \tag{3.3}$$

where $E[\cdot]$ represents the expected value or mean value. Mixed effects regression (e.g., Searle [1971]; Brillinger and Preisler [1985]; and Abrahamson and Youngs [1992)] is used to estimate the $ln(Sa_{RotD100}/Sa_{RotD50})$ while accounting for any earthquake-specific effects in the ratio of $Sa_{RotD100}$ and Sa_{RotD50}. The empirically computed geometric mean of $Sa_{RotD100}/Sa_{RotD50}$ from mixed-effects regression at different periods is shown in Figure 3.1.Table 3.1 shows the estimated $E\left[ln(Sa_{RotD100}/Sa_{RotD50})\right]$ along with the between-event standard deviation (τ) and within-event standard deviation (ϕ) (standard-deviation notation following Al Atik et al. [2010]). The low values of τ shows that the event terms for $ln(Sa_{RotD100}/Sa_{RotD50})$ are close to zero or the event terms for $lnSa_{RotD100}$ and $lnSa_{RotD50}$ are almost same as each other, and thus cancel out. This was expected, as the amplification/deamplification due to common source effects should be shared by both Sa_{RotD50} and $Sa_{RotD100}$. Results computed using different subsets of the NGA-West2 database used to develop other ground-motion models were found to be consistent with each other.

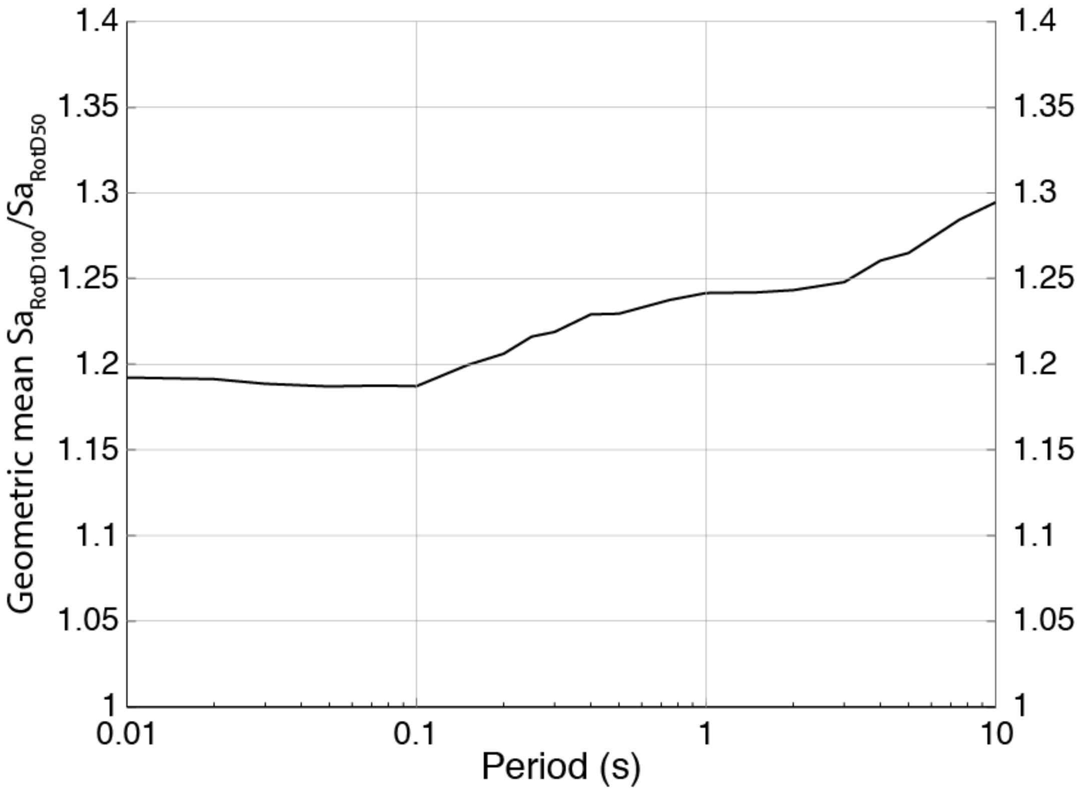

Figure 3.1 **Geometric mean of the observed ratio of $Sa_{RotD100}$ to Sa_{RotD50} estimated by mixed effects regression using NGA-West2 database.**

Table 3.1 **Fitted values of $ln(Sa_{RotD100}/Sa_{RotD50})$ with the within-event standard deviation (ϕ), between-event standard deviation (τ) and total standard deviation (σ), estimated by mixed effects regression. Note that the estimates are for mean of $ln(Sa_{RotD100}/Sa_{RotD50})$ and geometric mean of $Sa_{RotD100}/Sa_{RotD50}$ and the reported standard deviations are for $ln(Sa_{RotD100}/Sa_{RotD50})$ estimates.**

T(s)	$ln(\frac{Sa_{RotD100}}{Sa_{RotD50}})$	$\frac{Sa_{RotD100}}{Sa_{RotD50}}$	ϕ	τ	σ_{total}
0.01	0.176	1.19	0.08	0.01	0.08
0.02	0.175	1.19	0.08	0.01	0.08
0.03	0.172	1.19	0.08	0.01	0.08
0.05	0.171	1.19	0.08	0.01	0.08
0.075	0.172	1.19	0.08	0.01	0.08
0.1	0.172	1.19	0.08	0.01	0.08
0.15	0.182	1.20	0.08	0.01	0.08
0.2	0.187	1.21	0.08	0.01	0.08
0.25	0.196	1.22	0.08	0.01	0.08
0.3	0.198	1.22	0.08	0.01	0.08
0.4	0.206	1.23	0.08	0.01	0.08
0.5	0.206	1.23	0.09	0.01	0.09
0.75	0.213	1.24	0.08	0.01	0.08
1	0.216	1.24	0.08	0.01	0.08
1.5	0.217	1.24	0.08	0.01	0.08
2	0.218	1.24	0.08	0.01	0.08
3	0.221	1.25	0.08	0.01	0.08
4	0.231	1.26	0.08	0.01	0.08
5	0.235	1.26	0.08	0.02	0.08
7.5	0.251	1.28	0.08	0.02	0.08
10	0.258	1.29	0.07	0.03	0.08

3.1 COMPARISON WITH OTHER MODELS

Several researchers have computed estimates for the ratio of $Sa_{RotD100}$ to $Sa_{GMRotI50}$ in past (e.g., Beyer and Bommer [2006]; Watson-Lamprey and Boore [2007]; Campbell and Bozorgnia [2007, 2008]; and Huang et al. [2008, 2010]). To compare the older ratios of $Sa_{RotD100}$ to $Sa_{GMRotI50}$ with the $Sa_{RotD100}$ to Sa_{RotD50} ratios computed in this study, we use the factors proposed by Boore [2010] to convert the proposed $Sa_{RotD100}/Sa_{RotD50}$ ratios to $Sa_{RotD100}/Sa_{GMRotI50}$ ratios. Figure 3.1 compares our converted $Sa_{RotD100}$ to $Sa_{GMRotI50}$ ratios with previous results. Most of these models agree with each other in both the magnitude of the ratios and their trend with period. The one exception is the ratios proposed in NEHRP [2009] provisions.

The NEHRP [2009] $Sa_{RotD100}/Sa_{GMRotI50}$ ratios are based on the ratio of observed $Sa_{RotD100}$ values in recorded ground motions to the prediction of $Sa_{GMRotI50}$ by a ground-motion model. Modeling the ratio of an observed value to a predicted value—rather than the ratio of an observed value to an observed value—has some flaws. The NGA models were carefully fitted to provide an unbiased estimate of ground-motion intensity from future earthquakes [Abrahamson et al. 2008]. However, the dataset used to fit the ground-motion models is not an unbiased sample of earthquakes (e.g., there are many more ground motions from the 1999 M=7.6 Chi-Chi, Taiwan earthquake in the NGA database compared to other earthquakes). Statistical techniques such as mixed-effects regression have been used to overcome these biases in the dataset while fitting the NGA ground-motion models. The ratios recommended by NEHRP [2009] provisions effectively readjust the NGA ground-motion models, which undoes careful calculations that go into building a ground-motion model. For example, a particular earthquake can produce higher average ground-motion intensities than the unbiased ground-motion model estimate due to random chance (any effect not accounted for by the ground-motion model can be modeled as random chance). The ratios of observed $Sa_{RotD100}$ to the predicted Sa_{RotD50} for such an earthquake will be higher than the ratio of observed $Sa_{RotD100}$ to observed Sa_{RotD50}, as the first ratio will also include the random earthquake effect, which is carefully removed by the mixed effects regression used to fit ground-motion models. Modeling $Sa_{RotD100}/Sa_{RotD50}$ as the ratio of observed $Sa_{RotD100}$ to observed Sa_{RotD50}, and using the prediction from a ground-motion model as an estimate for $E[lnSa_{RotD50}]$ in Equation (3.3) allows us to leverage the results from careful fitting of ground-motion models and gives us a better estimate of $Sa_{RotD100}$ from a future earthquake.

Huang et al. [2008, 2010] reported that ground motion from Chi-Chi, Taiwan, earthquake had a significant effect on the geometric mean of the ratio of observed $Sa_{RotD100}$ to $Sa_{GMRotI50}$ values predicted by ground-motion models, so they reported different sets of results for datasets with and without the Chi-Chi records. As shown in Figure 3.2, we found that presence or absence of Chi-Chi records did not change significantly the geometric mean of observed $Sa_{RotD100}$ to observed Sa_{RotD50}. This indicates that the observed to observed ratio are more stable across different earthquake events compared to the observed to predicted ratio.

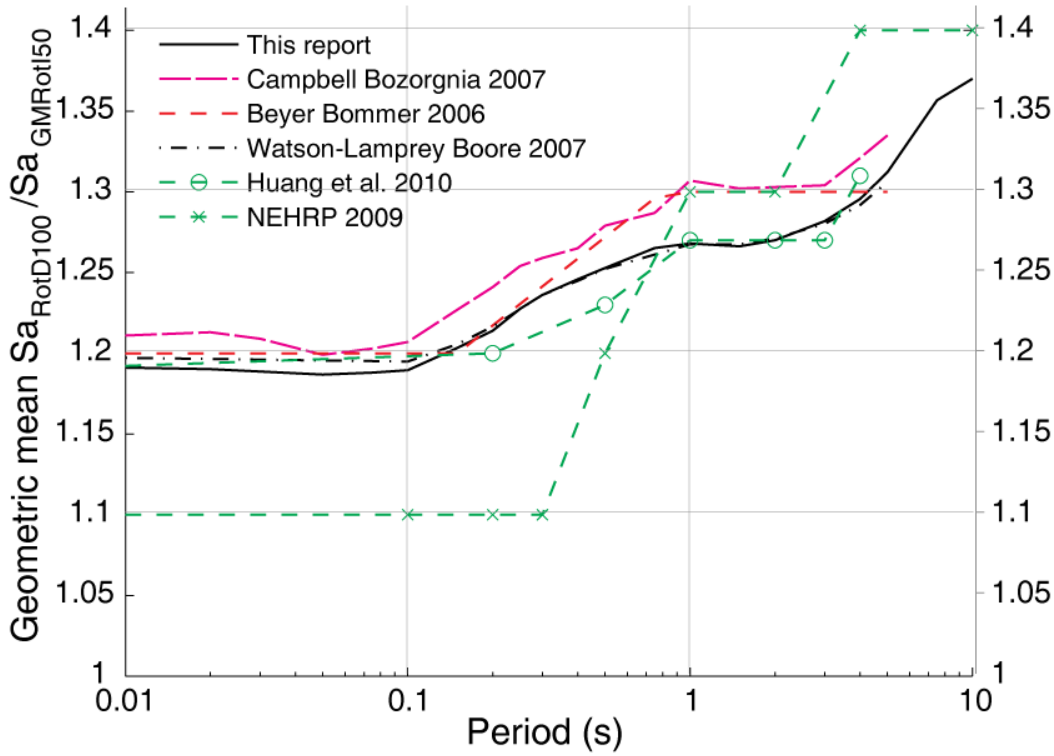

Figure 3.1 Comparison of various models for geometric mean $Sa_{RotD100}/Sa_{RotD50}$ ratios.

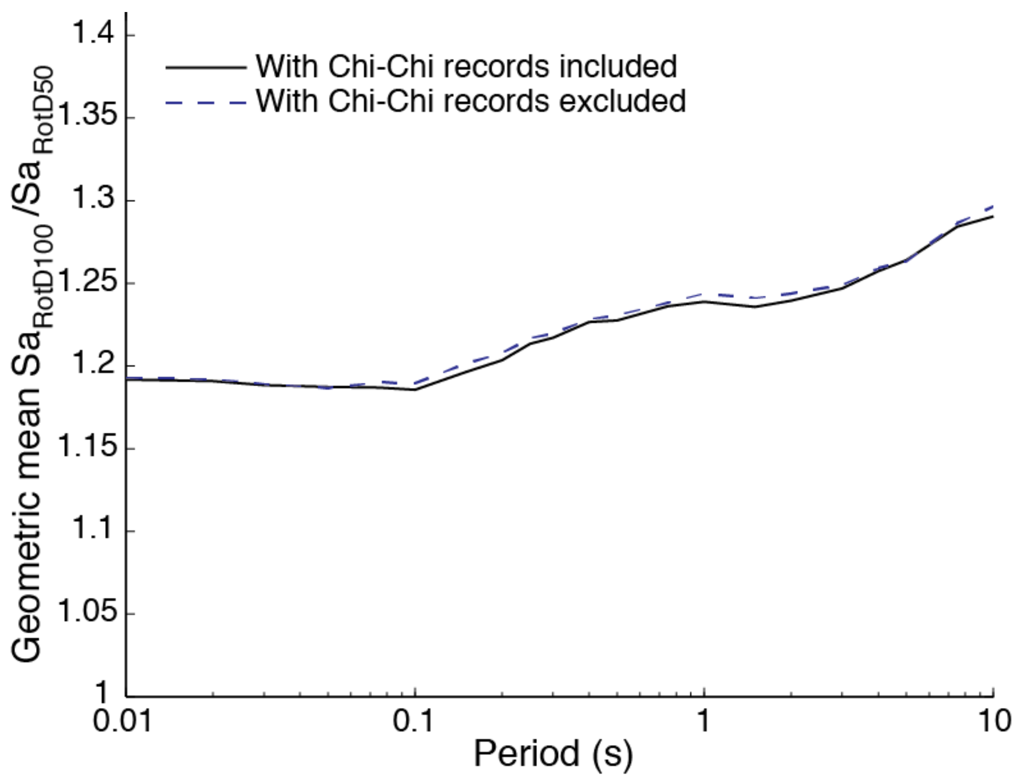

Figure 3.2 Comparison of the geometric means of $Sa_{RotD100}/Sa_{RotD50}$ estimated using datasets with and without the 1999 M=7.6 Chi-Chi ground motions.

3.2 DEPENDENCE OF $Sa_{RotD100}/Sa_{RotD50}$ ON OTHER PARAMETERS

Figure 2.2 and Figure 3.1 showed that the geometric mean value of $Sa_{RotD100}/Sa_{RotD50}$ depends on spectral acceleration period. We also investigated its dependence on other seismological parameters like earthquake magnitude, closest distance between source and the site and some directivity parameters. We studied the dependence of this ratio on other seismological parameters and fitted several regression models using variable selection techniques like forward selection, backward elimination, etc. After examining the practical and statistical significance of different models, we decided to develop a model for $ln(Sa_{RotD100}/Sa_{RotD50})$ that was a linear function of R_{rup} (closest distance between rupture and site). Other parameters such as magnitude, directivity predictor terms, etc., had no appreciable predictive power. Figures showing the weak dependence of $Sa_{RotD100}/Sa_{RotD50}$ on several seismological parameters are included in Appendix A. The linear model, shown in Equation (3.4) contains a coefficient a_0 that varies with period and a coefficient a_1 that is constant for all periods, and is estimated to be -1.614×10^{-4}. Coefficient a_0 is the same as the $ln(Sa_{RotD100}/Sa_{RotD50})$ values presented in Table 3.1

Note that this relationship was fitted using data with closest distance less than 200 km and over 90% of the data had closest distance less than 100 km. So, we do not recommend use of these models for distances larger than 200 km.

$$E\left[ln\left(\frac{Sa_{RotD100}}{Sa_{RotD50}}\right)\right] = a_0 + a_1\cdot(R_{rup} - 60) \tag{3.4}$$

The difference between the results from using a distance-dependent model or using a non-distance-dependent model is small, as can be seen in Figure 3.3. Thus, we report both the geometric mean of the ratio of $Sa_{RotD100}$ and Sa_{RotD50} and the coefficient a_0 from Equation (3.4) at different periods in Table 3.1. Either of the two models can be used depending on the level of precision required. This view is echoed in the similar earlier study by Watson-Lamprey and Boore [2007], who noted slight distance, magnitude and radiation pattern dependence, but stated that "for most engineering applications the conversion factors independent of those variables can be used." The results are reported at discrete set of periods and coefficients at other periods can be estimated by interpolating these results.

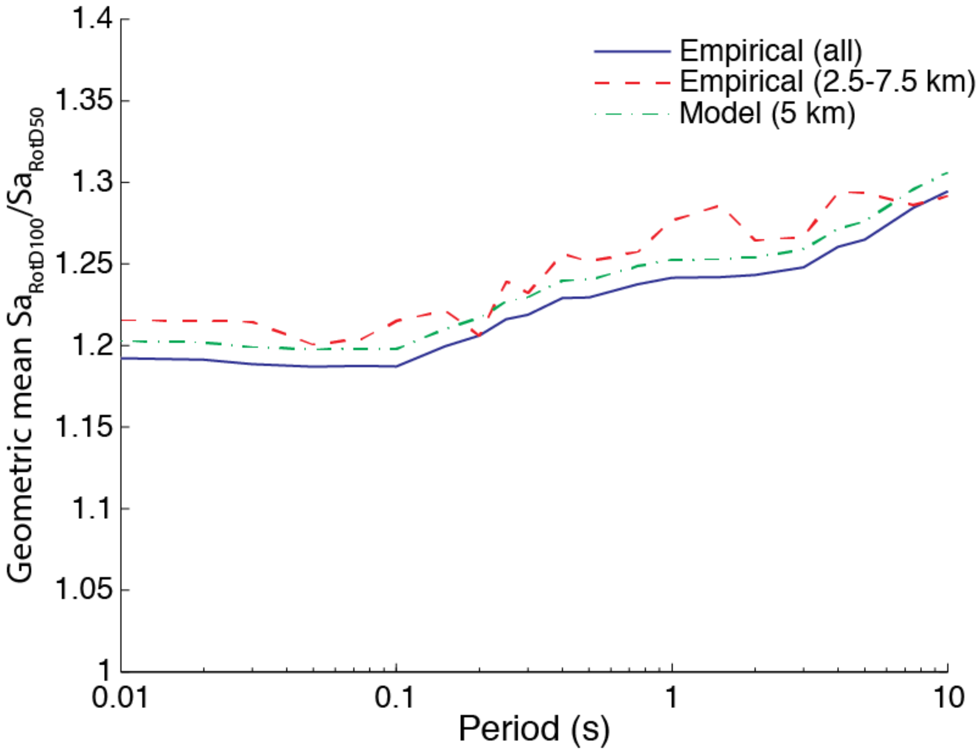

Figure 3.3 **Prediction of $Sa_{RotD100}/Sa_{RotD50}$ by the distance dependent model in Equation (3.4) for *R* = 5km, compared with the non-distance-dependent estimates of $Sa_{RotD100}/Sa_{RotD50}$ given in**

4 Orientation of $Sa_{RotD100}$

Structural systems generally have different resistance to seismic loads in different orientations. For these systems, the orientation in which the maximum spectral acceleration occurs is also important. We define the orientation of $Sa_{RotD100}$ as the minimum angle between the strike of the fault and the orientation of $Sa_{RotD100}$. This orientation, referred as α hereafter, ranges from 0 to 90° where $\alpha = 0$ represents the strike-parallel orientation and $\alpha = 90$ represent the strike-normal orientation.

To study these orientations, we computed α for each ground motion in our database at 21 periods, and then binned the data according to different seismological parameters and examined the distribution of α in each bin. Figure 4.1 shows the distribution of α in different M and R_{rup} bins. α is closer to the strike-normal orientation ($\alpha = 90$) more often than to the strike-parallel orientation ($\alpha = 0$) when the site is located within 5 km of the fault. On the other hand, when R_{rup} is greater than 5 km, α is almost uniformly distributed. The magnitude bins do not seem to have any significant influence on the distribution of α. To examine the effect of period on $Sa_{RotD100}$ orientation (α), we binned all the data within 5 km of the fault by period. Histograms of α in different period bins are shown in Figure 4.2. The distribution of α is nearly uniform for periods less than 1 sec, while orientations close to strike-normal are more frequent than strike-parallel for periods larger than 1 sec.

After examining histograms of α binned by several parameters (two other examples are shown in Appendix B), we decided to model the distribution of α as uniform for sites when R_{rup} is greater than 5 km or when the spectral-acceleration period under consideration is less than 1 sec. For other cases ($R_{rup} < 5$ km and $T \geq 1$ sec) the data was pooled and the distribution was modeled empirically by counting the number of α observed in 10° bins. This empirically computed distribution is presented in Table 4.1.

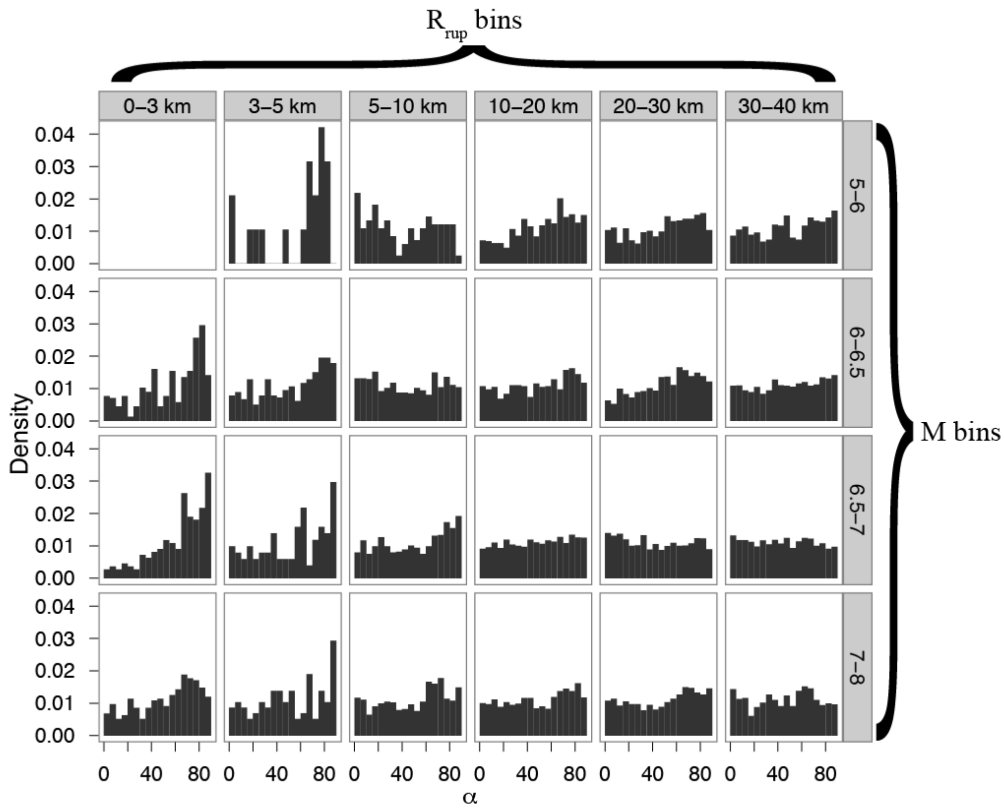

Figure 4.1 Probability density of α ($Sa_{RotD100}$ orientations) in different M, R_{rup} bins.

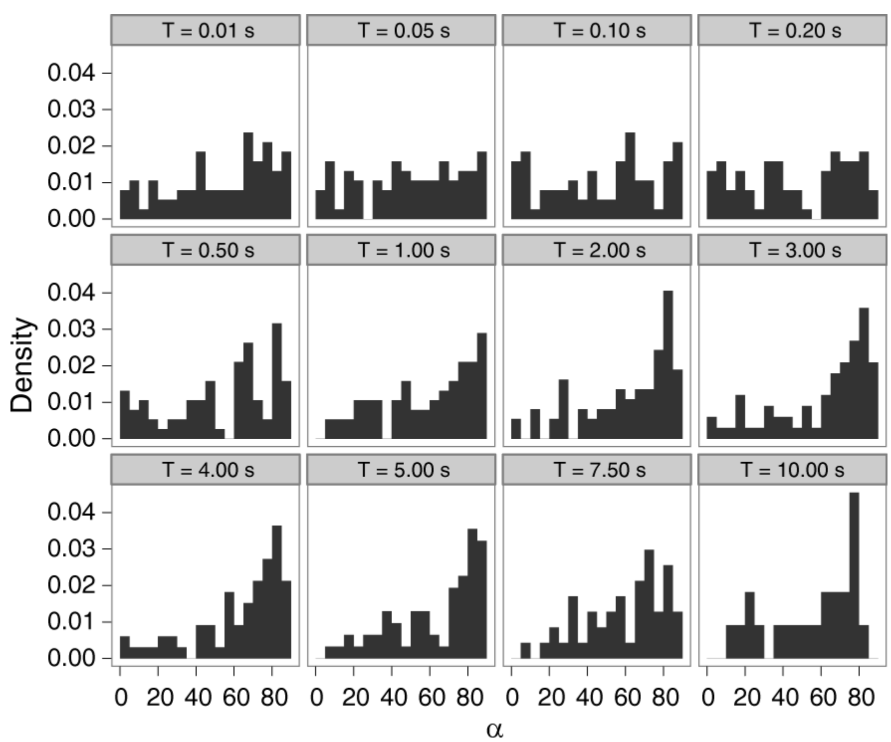

Figure 4.2 Probability density of α for sites with R_{rup} < 5 km, binned by period (sec).

Table 4.1 Probability density of α for R_{rup} < 5 km and $T \geq$ 1 sec.

Orientations (degrees)	Probability
0-10	0.031
10-20	0.055
20-30	0.070
30-40	0.067
40-50	0.080
50-60	0.100
60-70	0.106
70-80	0.233
80-90	0.258

4.1 RELATIONSHIP BETWEEN $Sa_{RotD100}$ ORIENTATIONS AT DIFFERENT PERIODS

Figure 4.3 shows the polarization of displacement response and orientation of $Sa_{RotD100}$ intensity from an example ground motion at two different periods (say T^* and T'). The $Sa_{RotD100}$ intensity at different periods may occur in different orientations and the difference in orientation ($|\alpha^* - \alpha'|$ in Figure 4.3) can be used to study the relationship between the $Sa_{RotD100}$ orientations at different periods. This knowledge can be used to construct more realistic single orientation target spectra, as shown below.

The difference in the orientation of $Sa_{RotD100}$ at two periods has a lot of uncertainty and can take any value between 0° (i.e., the orientation at both period are the same) to 90° (i.e., the $Sa_{RotD100}$ occurs in orthogonal orientations at the two periods). Figure 4.4 shows the histogram of the difference in $Sa_{RotD100}$ orientation ($|\alpha^* - \alpha'|$) at two different periods. The probability distribution of $|\alpha^* - \alpha'|$ depends on the periods under consideration $|\alpha^* - \alpha'|$ is more likely to be close to 0° when the periods are closer to each other. Thus, the average difference between the orientations increases with increasing difference between the periods.

After examining histograms at several sets of periods, the truncated exponential distribution was selected to model the distribution of $|\alpha^* - \alpha'|$. The truncated exponential distribution is described below

$$f(x) = \begin{cases} \dfrac{\lambda e^{-\lambda x}}{1-e^{-90\lambda}}; & x \leq 90 \\ 0 & \text{otherwise} \end{cases} \tag{4.1}$$

The distribution depends on the parameter λ, which is estimated here using the maximum likelihood method. The estimated parameters are presented in Table 4.2. When $T^* = T'$, $\lambda \to \infty$, and thus the probability density becomes a Dirac-delta function centered at 0°. Figure 4.4 shows the comparison of the fitted distribution with empirical histograms for two periods.

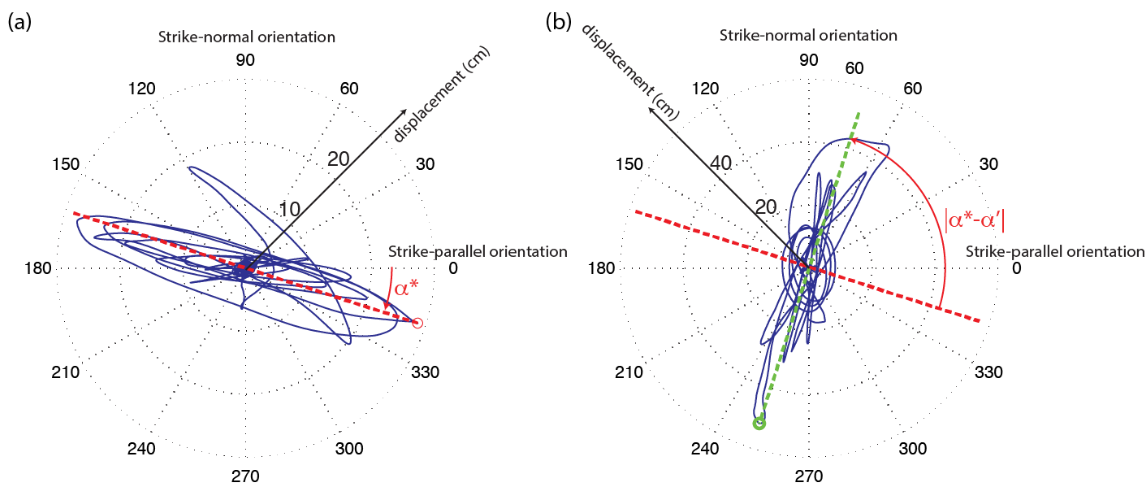

Figure 4.3 **Displacement response trace to the El Centro Differential Array recording from the 1979 Imperial Valley earthquake. The period of the SDOF oscillator is (a) T^* = 1.5 sec and (b) T' = 3 sec. The orientations of $Sa_{RotD100}$ along with the difference between these orientations at the two periods ($|\alpha^* - \alpha'|$) is also shown.**

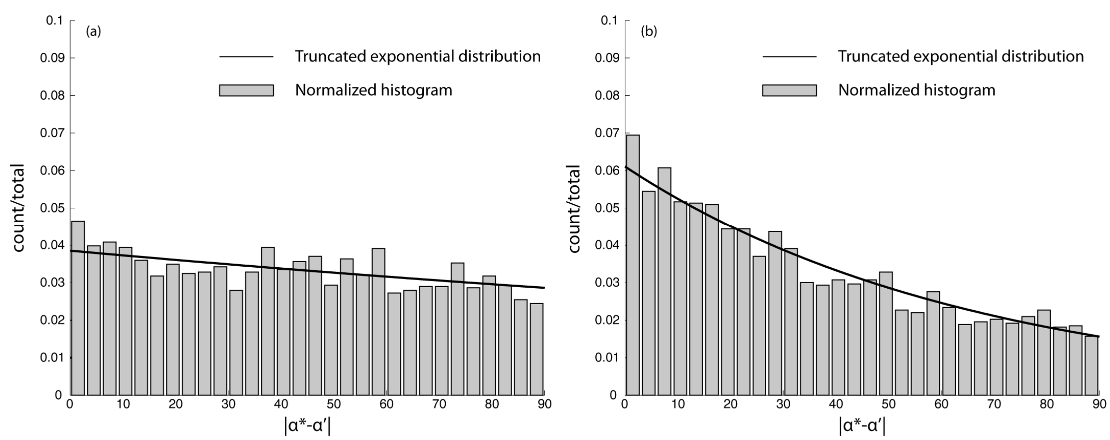

Figure 4.4 **Distribution of $|\alpha^* - \alpha'|$ as predicted by the truncated exponential model is compared with the normalized histogram for a) T^* = 2 sec and T' = 0.1 sec and b) T^* = 2 sec and T' = 1 sec.**

Table 4.2 **Estimated values of the parameter λ for the truncated exponential model. The table is symmetric, or coefficient at row i and column j and coefficient at row j and column i are same; therefore, only half of the coefficients are shown.**

		T^*										
		0.01	**0.02**	**0.03**	**0.05**	**0.07**	**0.10**	**0.15**	**0.20**	**0.25**	**0.30**	**0.40**
	0.01	∞										
	0.02	0.579	∞									
	0.03	0.186	0.188	∞								
	0.05	0.070	0.071	0.072	∞							
	0.07	0.042	0.042	0.042	0.041	∞						
	0.10	0.031	0.031	0.030	0.028	0.031	∞					
	0.15	0.022	0.022	0.022	0.020	0.019	0.020	∞				
	0.20	0.021	0.021	0.021	0.019	0.017	0.015	0.019	∞			
	0.25	0.020	0.019	0.019	0.17	0.016	0.014	0.013	0.021	∞		
	0.30	0.020	0.020	0.019	0.017	0.016	0.014	0.013	0.016	0.026	∞	
T'	**0.40**	0.020	0.020	0.020	0.016	0.015	0.011	0.010	0.013	0.015	0.019	∞
	0.50	0.018	0.018	0.018	0.015	0.013	0.011	0.009	0.011	0.010	0.013	0.024
	0.75	0.014	0.014	0.013	0.012	0.010	0.009	0.006	0.007	0.007	0.007	0.011
	1.00	0.013	0.013	0.012	0.010	0.009	0.007	0.005	0.005	0.005	0.007	0.010
	1.50	0.010	0.010	0.009	0.007	0.007	0.005	0.003	0.003	0.004	0.005	0.008
	2.00	0.007	0.007	0.007	0.006	0.005	0.003	0.002	0.003	0.004	0.003	0.005
	3.00	0.004	0.004	0.004	0.004	0.003	0.003	0.000	0.001	0.003	0.004	0.004
	4.00	0.005	0.005	0.006	0.005	0.004	0.003	0.001	0.002	0.003	0.004	0.006
	5.00	0.007	0.007	0.007	0.005	0.004	0.003	0.002	0.003	0.003	0.005	0.007
	7.50	0.007	0.007	0.007	0.006	0.004	0.003	0.002	0.002	0.003	0.004	0.005
	10.00	0.007	0.007	0.007	0.005	0.005	0.003	0.002	0.002	0.003	0.005	0.005

		T^*									
		0.50	0.70	1.00	1.50	2.00	3.00	4.00	5.00	7.50	10.0
	0.01										
	0.02										
	0.03										
	0.05										
	0.07										
	0.10										
	0.15										
	0.20										
	0.25										
	0.30										
T'	0.40										
	0.50	∞									
	0.75	0.016	∞								
	1.00	0.013	0.022	∞							
	1.50	0.008	0.013	0.020	∞						
	2.00	0.007	0.011	0.015	0.024	∞					
	3.00	0.004	0.006	0.010	0.012	0.019	∞				
	4.00	0.005	0.008	0.010	0.011	0.016	0.029	∞			
	5.00	0.005	0.009	0.010	0.012	0.015	0.024	0.040	∞		
	7.50	0.005	0.009	0.011	0.013	0.016	0.019	0.025	0.034	∞	
	10.00	0.005	0.009	0.010	0.013	0.014	0.017	0.021	0.027	0.057	∞

5 *Sa* at Arbitrary Orientations

A model to predict *Sa* in an arbitrary orientation is needed to compute single orientation conditional spectra. Here we study the Sa in an orientation $\phi°$ away from the $Sa_{RotD100}$ orientation. This *Sa* is referred hereafter as Sa_{ϕ}. An empirical model for the ratio of Sa_{ϕ}/Sa_{RotD50} is developed, which can be used as a multiplicative factor with a ground-motion model prediction of Sa_{RotD50} to get a prediction for Sa_{ϕ}. The spectral acceleration in each orientation was computed for all the ground-motion recordings used in this study. This dataset was used to empirically compute the geometric mean of the Sa_{ϕ}/Sa_{RotD50}. As the event terms from mixed effects regression for $ln(Sa_{RotD100}/Sa_{RotD50})$ were found to be close to 0, we ignored the inter-event terms and pooled the data across different earthquakes, and estimated the Sa_{ϕ}/Sa_{RotD50} using geometric means of the pooled data. The $Sa_{RotD100}/Sa_{RotD50}$ values estimated using mixed effects regression (Table 3.1) and empirical geometric means (values corresponding to $\phi = 0$ in Table 5.1) vary slightly but are practically identical.

Figure 5.1 shows the modeled ratio for three different periods. As expected the ratio is highest at $\phi = 0$, where it is same as $Sa_{RotD100}$, and decreases with increase of ϕ. Table 5.1 presents the geometric mean of Sa_{ϕ}/Sa_{RotD50} at ϕ values from 0 to 90°at 5° intervals for 21 periods. Predictions at other periods and ϕ values can be found by interpolating these results.

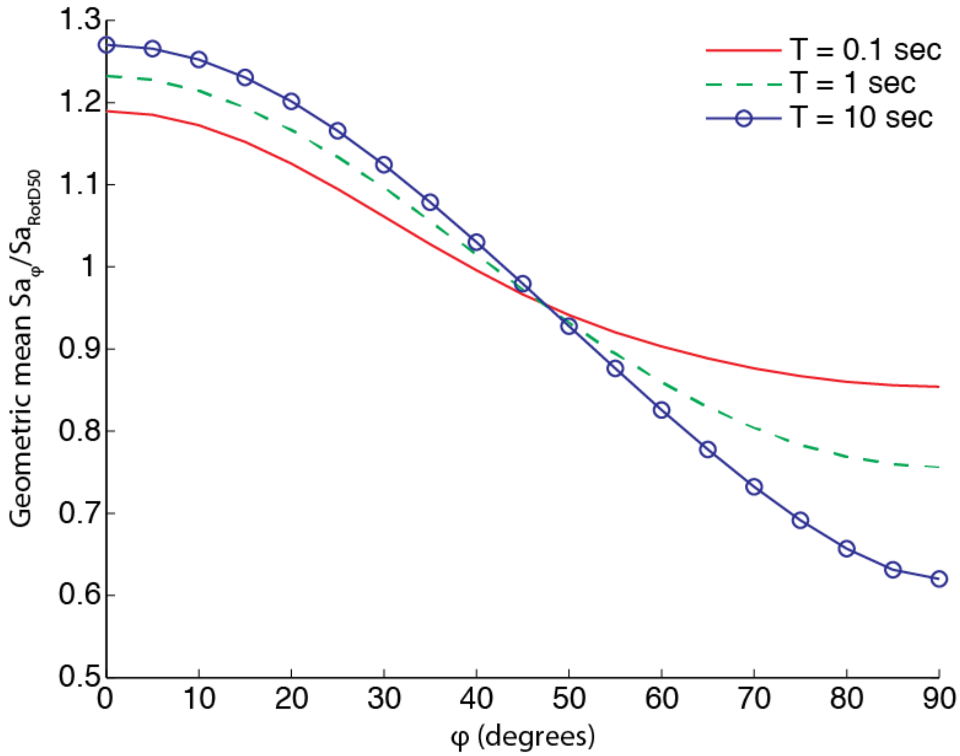

Figure 5.1 **The geometric mean of Sa_ϕ/Sa_{RotD50} as a function of ϕ for different periods.**

Table 5.1 Geometric mean of Sa_{ϕ}/Sa_{RotD50} at various values of ϕ and T.

		$\phi(degrees)$									
		0	**5**	**10**	**15**	**20**	**25**	**30**	**35**	**40**	**45**
T'	**0.01**	1.192	1.188	1.175	1.154	1.127	1.096	1.061	1.026	0.993	0.963
	0.02	1.191	1.187	1.174	1.154	1.127	1.095	1.061	1.026	0.993	0.964
	0.03	1.188	1.184	1.171	1.151	1.124	1.093	1.059	1.025	0.992	0.963
	0.05	1.187	1.183	1.170	1.150	1.123	1.091	1.058	1.024	0.992	0.964
	0.07	1.187	1.183	1.170	1.150	1.123	1.091	1.058	1.024	0.992	0.965
	0.10	1.186	1.181	1.168	1.148	1.122	1.091	1.058	1.024	0.993	0.965
	0.15	1.196	1.192	1.179	1.159	1.133	1.101	1.067	1.032	0.998	0.967
	0.20	1.204	1.199	1.187	1.166	1.140	1.109	1.074	1.038	1.003	0.968
	0.25	1.213	1.209	1.196	1.176	1.149	1.117	1.082	1.044	1.006	0.969
	0.30	1.217	1.213	1.200	1.180	1.153	1.120	1.084	1.046	1.008	0.970
	0.40	1.227	1.222	1.209	1.189	1.162	1.129	1.093	1.053	1.013	0.972
	0.50	1.228	1.223	1.210	1.190	1.163	1.130	1.094	1.054	1.013	0.972
	0.75	1.236	1.232	1.219	1.198	1.171	1.138	1.100	1.059	1.017	0.974
	1.00	1.239	1.234	1.222	1.201	1.173	1.140	1.102	1.061	1.017	0.973
	1.50	1.236	1.231	1.219	1.198	1.171	1.138	1.100	1.059	1.016	0.973
	2.00	1.240	1.235	1.222	1.201	1.174	1.140	1.102	1.061	1.018	0.974
	3.00	1.247	1.243	1.229	1.209	1.180	1.146	1.108	1.066	1.021	0.975
	4.00	1.257	1.253	1.240	1.219	1.190	1.156	1.116	1.073	1.026	0.977
	5.00	1.264	1.259	1.246	1.225	1.196	1.161	1.121	1.077	1.029	0.979
	7.50	1.284	1.280	1.266	1.245	1.215	1.180	1.138	1.091	1.039	0.985
	10.00	1.290	1.286	1.272	1.250	1.221	1.184	1.141	1.093	1.041	0.985

		$\phi (degrees)$								
		50	**55**	**60**	**65**	**70**	**75**	**80**	**85**	**90**
	0.01	0.939	0.919	0.903	0.891	0.882	0.874	0.869	0.865	0.864
	0.02	0.939	0.920	0.904	0.892	0.882	0.875	0.869	0.866	0.865
	0.03	0.940	0.921	0.906	0.893	0.884	0.877	0.872	0.868	0.867
	0.05	0.941	0.923	0.908	0.896	0.887	0.880	0.874	0.871	0.870
	0.07	0.942	0.923	0.908	0.896	0.887	0.879	0.874	0.871	0.870
	0.10	0.941	0.922	0.906	0.893	0.882	0.874	0.868	0.865	0.864
	0.15	0.939	0.915	0.895	0.880	0.867	0.858	0.851	0.847	0.845
	0.20	0.938	0.910	0.887	0.869	0.854	0.843	0.835	0.830	0.829
	0.25	0.935	0.905	0.879	0.858	0.841	0.828	0.819	0.813	0.812
	0.30	0.935	0.902	0.874	0.850	0.830	0.814	0.803	0.796	0.794
T'	**0.40**	0.934	0.899	0.868	0.841	0.819	0.802	0.789	0.781	0.779
	0.50	0.933	0.896	0.863	0.835	0.811	0.792	0.780	0.773	0.770
	0.75	0.933	0.893	0.857	0.825	0.798	0.776	0.761	0.752	0.749
	1.00	0.931	0.891	0.854	0.822	0.795	0.773	0.757	0.748	0.745
	1.50	0.932	0.892	0.855	0.823	0.795	0.773	0.757	0.748	0.744
	2.00	0.930	0.889	0.851	0.817	0.789	0.766	0.750	0.740	0.737
	3.00	0.929	0.885	0.845	0.809	0.778	0.753	0.734	0.723	0.719
	4.00	0.929	0.881	0.837	0.796	0.761	0.730	0.708	0.693	0.688
	5.00	0.928	0.877	0.828	0.781	0.740	0.704	0.677	0..658	0.652
	7.50	0.928	0.869	0.810	0.753	0.699	0.650	0.608	0.577	0.565
	10.00	0.927	0.867	0.806	0.746	0.688	0.635	0.589	0.555	0.542

6 Example Target Spectra

As discussed above, the $Sa_{RotD100}$ spectrum is an envelope over spectra from all orientations at each period. Figure 4.3 shows that the $Sa_{RotD100}$ value may be observed in very different orientations, even at two periods which are close to each other. So, it is very unlikely to observe $Sa_{RotD100}$ at multiple periods in a single orientation. Thus, using $Sa_{RotD100}$ as a target design spectrum may result in conservative estimates of engineering demand parameters (EDPs), which depends on multiple periods (e.g., peak floor acceleration, interstory drift ratio, etc.). Conditional mean spectra approach (e.g., Baker [2011]) can be used to compute more realistic single orientation target spectra for design.

The conditional mean spectrum is the expected value of the ground-motion intensity conditioned upon some information. Here we study the computation of two such target spectra conditioned on a specific orientation and on a $Sa_{RotD100}$ observation in a specific period.

6.1 SPECTRA CONDITIONED ON ORIENTATION

Structures generally have different load resistance in different orientations. If some orientation is more important than other orientations, then the expected value of Sa in that particular orientation can be used as an appropriate target spectrum. Since this response spectrum is conditioned on a single orientation it does not suffer from the problem of having Sa from different orientations at different periods, as in case of the $Sa_{RotD100}$ spectra.

The target spectrum conditioned on an orientation, $\theta°$ away from strike-parallel orientation can be computed using the equation below

$$\begin{aligned} E[Sa \mid \theta] &= \int_0^{90} E[Sa_\theta \mid \alpha] \cdot P(\alpha) d\alpha \\ &= \int_0^{90} E[Sa_{\theta-\alpha}] \cdot P(\alpha) d\alpha \\ &= \int_0^{90} \frac{Sa_{\theta-\alpha}}{Sa_{RotD50}} \cdot \hat{S}a_{RotD50} \cdot P(\alpha) d\alpha \end{aligned} \tag{6.1}$$

where $\boldsymbol{\alpha}$ represents the orientation in which the $\boldsymbol{Sa_{RotD100}}$ is observed at the period for which computation is being done and $\boldsymbol{\widehat{Sa}_{RotD50}}$ represents the $\boldsymbol{Sa_{RotD50}}$ prediction from a ground-motion model.

Table 5.1 gives the values of $Sa_{\theta-\alpha}/Sa_{RotD50}$ at different periods and $\phi = \theta - \alpha$ orientations. While Table 4.1 describes the probability distribution of α [i.e. $P(\alpha)$].

Spectra conditioned in the strike-normal and strike-parallel orientations are compared with corresponding Sa_{RotD50} and $Sa_{RotD100}$ in Figure 6.1. These computations were done for an earthquake of magnitude 7, at a site with a V_{S30} of 760m/sec, and located 2.5 km away from the rupture. The Boore and Atkinson [2008] model prediction was used to estimate Sa_{RotD50} [i.e., $\widehat{Sa}_{RotD50}$ in Equation (6.1)]. It should be noted that Boore and Atkinson [2008] model gives prediction for $Sa_{GMRotI50}$ intensity, and conversion factors from Boore [2010] were used to convert the $Sa_{GMRotI50}$ intensities to Sa_{RotD50}.

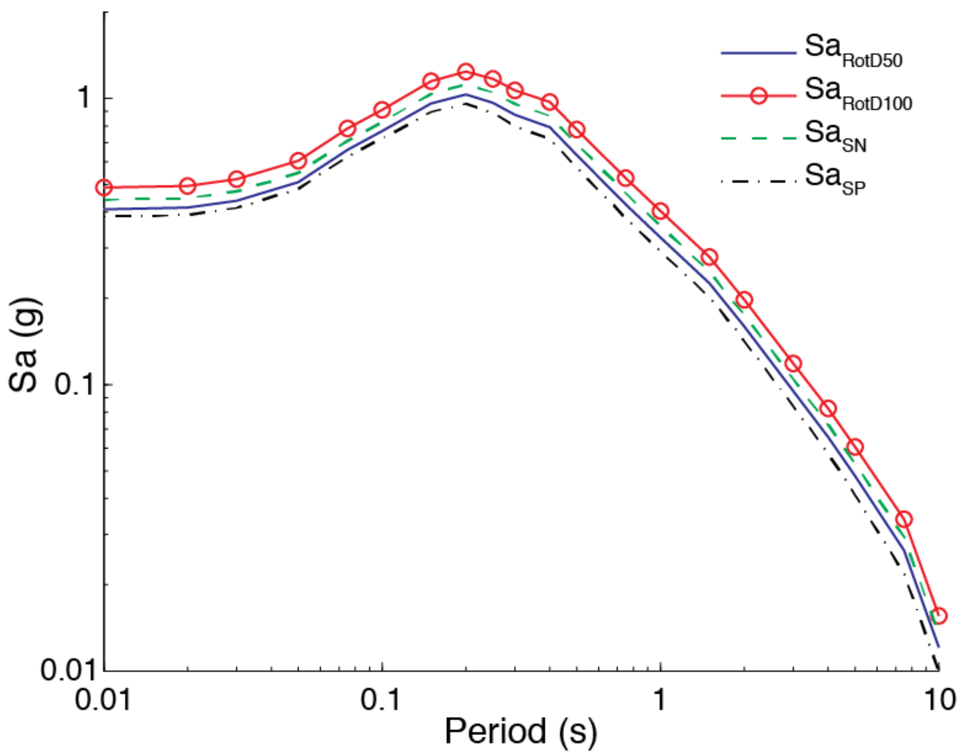

Figure 6.1 **Comparison of the median predicted $Sa_{RotD100}$ and Sa_{RotD50} spectra with spectra conditioned in strike-normal and strike-parallel orientations. All results are for an earthquake with magnitude 7, at distance of 2.5 km, and with a V_{S30}= 760 m/sec.**

6.2 SPECTRA CONDITIONED ON THE ORIENTATION OF $Sa_{RotD100}$ AT A GIVEN PERIOD

Since, the orientation of $Sa_{RotD100}$ is random, the spectrum conditioned on a single orientation can never be as large as $Sa_{RotD100}$ at any period. Structural response is often primarily driven by the ground-motion intensity at a single period. Thus, if a single period is more important than others, a more appropriate target spectrum could be the one conditioned on the orientation in which $Sa_{RotD100}$ is observed at the important period (say T^*). If the spectrum is conditioned on

$Sa_{RotD100}$ orientation at the period T^* (i.e., orientation = α^*), the expected value of the Sa at a different period, say T', can be computed using Equation (6.2):

$$\begin{aligned} E[SaT' \mid \alpha^*] &= \int_0^{90} E[SaT' \mid \alpha', \alpha^*] P(\alpha' \mid \alpha^*) d\alpha' \\ &= \int_0^{90} E[SaT'_{|\alpha^*-\alpha'|} \mid \alpha', \alpha^*] P(|\alpha' - \alpha^*|) d\alpha' \\ &= \int_0^{90} \frac{Sa_{\alpha^*-\alpha'}}{Sa_{RotD50}} \cdot \hat{S}a_{RotD50} P(|\alpha' - \alpha^*|) d\alpha' \end{aligned} \tag{6.2}$$

where $\frac{Sa_{\alpha^*-\alpha'}}{Sa_{RotD50}}$ is given by Table 5.1 for different values of $\phi = |\alpha^* - \alpha'|$ and periods (T'). $\widehat{Sa}_{RotD50}$ is the prediction from a ground-motion model and $P(|\alpha' - \alpha^*|)$ is modeled by the truncated exponential distribution with the parameter λ for the pair of periods T' and T^* given in Table 4.2.

Spectra conditioned on the $Sa_{RotD100}$ orientations at T^* = 0.2 sec and T^* = 1 sec are compared with the Sa_{RotD50} and $Sa_{RotD100}$ in Figure 6.2. These computations were done for an earthquake of magnitude 7, at a site with a V_{S30} of 760m/sec, and located 2.5 km away from the rupture. Again the Boore and Atkinson [2008] model prediction was used to estimate Sa_{RotD50}.

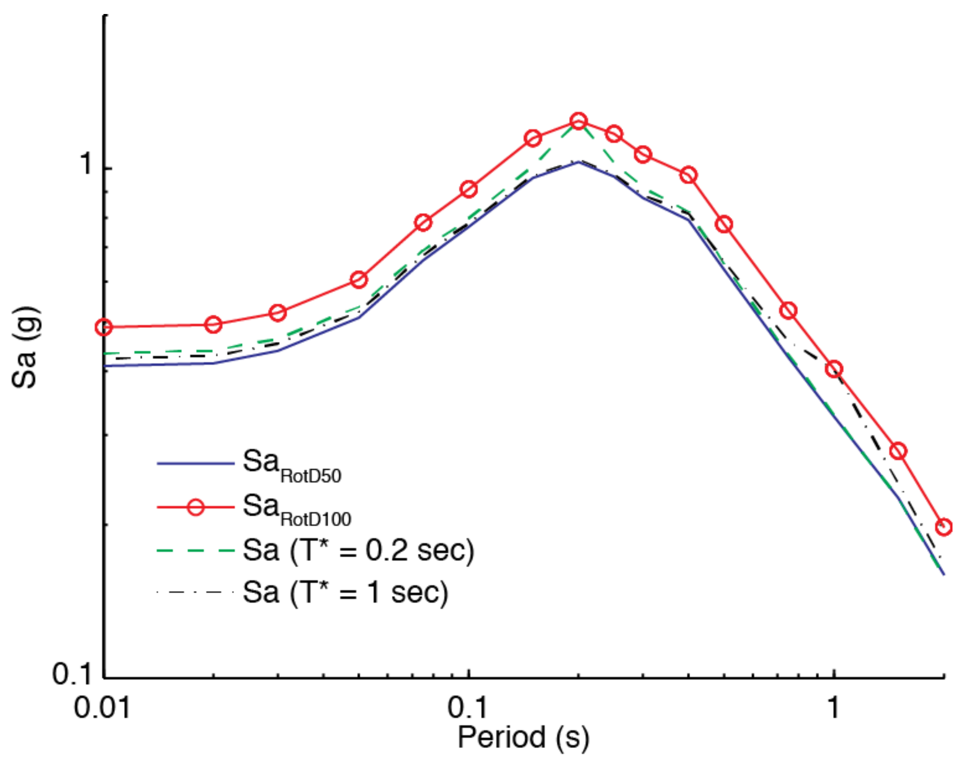

Figure 6.2 **Comparison of the $Sa_{RotD100}$ and Sa_{RotD50} spectra with spectra conditioned on $Sa_{RotD100}$ orientation at T^* = 0.2 sec and T^* = 1 sec. All results are for an earthquake with magnitude 7, at distance of 2.5 km, and a V_{S30} = 760 m/sec.**

7 Conclusions

In this study, we examined different methods of representing the intensity of ground motion in the horizontal plane using a response spectrum that is a one-dimensional representation of ground-motion intensity. We focused on two orientation-independent representations of the response spectrum: Sa_{RotD50} and $Sa_{RotD100}$. The new ground-motion models being developed as part of the NGA-West2 project will predict the Sa_{RotD50} spectrum at a site due to a future earthquake, while the NEHRP [2009] provisions recommend using $Sa_{RotD100}$ for seismic design. We have proposed a model to predict the ratio of $Sa_{RotD100}$ to Sa_{RotD50}, which can be used as a multiplicative factor with the Sa_{RotD50} predictions from the new NGA-West2 ground-motion models to predict the $Sa_{RotD100}$ ground-motion intensity. The proposed model was compared and was found to be consistent with similar models built in the past, though the proposed model advances that earlier work by using a larger data set, utilizing the recently adopted Sa_{RotD50} definition instead of $Sa_{GMRotI50}$ and using mixed effects regression to account for inter-event terms. The differences between the proposed model and corresponding NEHRP [2009] ratios were also explained. One important observation from this work is that the current NEHRP ratio of 1.1 at small periods is incorrect and should be approximately 1.2; this result is confirmed by other studies, as was illustrated in Figure 3.2.

Along with modeling the ratio of $Sa_{RotD100}$ to Sa_{RotD50}, we also modeled the probability distribution of orientations in which the $Sa_{RotD100}$ intensity is observed relative to the strike of the fault. The orientations of $Sa_{RotD100}$ were observed to be uniformly distributed when the closest distance between the fault and the site was greater than 5 km, or if the period under consideration was less than 1 sec. Only for the cases when the site was within 5 km of the fault and at periods greater than 1 sec, the orientation of $Sa_{RotD100}$ was more likely to be closer to the strike-normal than strike-parallel direction. The relationship between the orientations of $Sa_{RotD100}$ at different periods was also studied, and the difference between the orientation was modeled using a truncated exponential distribution. Together these models can help solve a practical problem of converting between two important IMs while helping deepen the understanding of the directionality of ground motions by studying the distribution of orientations in which $Sa_{RotD100}$ occurs and dependence of the $Sa_{RotD100}$ to Sa_{RotD50} ratio on different seismological parameters. Spectra conditioned on an orientation and on the orientation in which $Sa_{RotD100}$ is observed at a particular period were discussed. Example computations of these spectra using the models developed in the study were also presented.

It is anticipated that these results will help bridge the gap between the work of seismic hazard analysts, who typically use Sa_{GM} or Sa_{RotD50} values, and design engineers, some of whom prefer to work with $Sa_{RotD100}$ response spectra.

8 Recommendations for Future Research

This report summarizes a comprehensive study of ground-motion directionality in accordance with the original goals of the NGA-West2 project. The study nonetheless raised some questions which were not resolved, and would benefit from future research as summarized below.

8.1 PHYSICS OF DIRECTIONALITY AND CONNECTIONS TO DIRECTIVITY

Though this report focuses on the statistical study of ground-motion directionality, the results raise important questions about the physical process behind ground-motion directionality. Most importantly, the results show that the connection between directivity and directionality may be weaker than intuitively expected. Directivity (in the context of S-waves) can cause preferential polarization of ground motion in the fault normal orientation, but directivity effects are not equally strong at all periods, fault distances, and orientations with respect to the fault. While the directionality effects studied here are remarkably uniform over variations in those conditions, as can be seen in Figures A.1 to A.8, directivity causes polarization in approximately fault-normal orientations; however, this study showed that there is no preferential orientation of $Sa_{RotD100}$ beyond 5 km of the fault. Even within km of the fault, the fault-normal polarization is weaker than that expected from directivity. Additionally, the $Sa_{RotD100}/Sa_{RotD50}$ ratios and the $Sa_{RotD100}$ orientations do not show any significant trend with directivity parameters (e.g., IDP and ξ), as shown in Appendix A. In summary, occurrence of high $Sa_{RotD100}/Sa_{RotD50}$ ratios does not appear to be related to occurrence of directivity; therefore, the directionality models proposed here do not account for the impact of directivity on ground motions. Many of these observations were first noted by Watson-Lamprey and Boore [2007], and they suggest that further research is needed to describe the physical processes, if any, behind ground-motion directionality.

8.2 INPUT GROUND MOTIONS FOR NONLINEAR DYNAMIC ANALYSIS

Target response spectra are used widely in earthquake engineering, both as targets for ground-motion selection and scaling, or for other related assessment procedures. Engineering codes and technical groups have recently debated at length the relative merits of using Sa_{RotD50} or $Sa_{RotD100}$ to define a target spectrum. Two related conditional target spectra were suggested in this study, but their impact on results from engineering analyses was not considered. Further study is required to evaluate the impact of using different target spectra considered herein. Some results from the study raise interesting questions about the orientation in which selected ground-motions should be input to a dynamic analysis model. Damage is driven by a variety of response parameters, (e.g., story drift ratios, floor accelerations) and different parameters are generally sensitive to spectral acceleration at different periods. Results from this study show that the orientation of maximum Sa frequently differs with period. It is not clear which orientation of the input ground-motion causes maximum damage when damage is sensitive to a range of periods, and there is ongoing debate regarding how to use $Sa_{RotD100}$ to select and scale motions in a manner that reflects properties of real ground motions. Further research on these topics would be useful for developing recommendations that utilize our current knowledge of directionality.

REFERENCES

Abrahamson N., Youngs R.R. (1992). A stable algorithm for regression analysis using the random effects model, Bull. Seismol. Soc. Am., 82(1): 505–510.

Abrahamson N. (1998). Statistical properties of peak ground accelerations recorded by the SMART 1 array, Bull. Seismol. Soc. Am., 78(1): 26–41.

Abrahamson N., Atkinson G., Boore D.M, Bozorgnia Y., Campbell K., Chiou B., Idriss I.M., Silva W.J., Youngs R.R. (2008). Comparisons of the NGA ground-motion relations, Earthq. Spectra, 24(1): 45–66.

Al Atik L., Abrahamson N., Bommer J.J., Scherbaum F., Cotton F., Kuehn N. (2010). The variability of ground-motion prediction models and its components, Seismol. Res. Lett., 81(5), 794-801.

Baker J.W. (2011). The conditional mean spectrum: a tool for ground motion selection, J. Struct. Eng., 137(3): 322–331.

Baker J.W., Cornell C.A. (2006). Which spectral acceleration are you using? Earthq. Spectra 22(2): 293–312.

Beyer K., Bommer J.J. (2006). Relationships between median values and between aleatory variabilities for different definitions of the horizontal component of motion, Bull. Seismol. Soc. Am., 96(4A): 1512–1522.

Boore D.M. (2010). Orientation-independent, nongeometric-mean measures of seismic intensity from two horizontal components of motion, Bull. Seismol. Soc. Am., 100(4): 1830–1835.

Boore D.M., Atkinson G.M. (2008). Ground-motion prediction equations for the average horizontal component of PGA, PGV, and 5%-damped PSA at spectral periods between 0.01 s and 10.0 s, Earthq. Spectra, 24(1): 99–138.

Boore D.M., Watson-Lamprey J., Abrahamson N.A. (2006). Orientation-independent measures of ground motion, Bull. Seismol. Soc. Am., 96(4A): 1502–1511.

Bozorgnia, Y., N. Abrahamson, K. Campbell, B. Rowshandel, and T. Shantz (2012). NGA-West2: A comprehensive research program to update ground motion prediction equations for shallow crustal earthquakes in active tectonic regions. In 15th Word conference on earthquake engineering, Lisbon, Portugal, 6pp.

Brillinger D.R., Preisler H.K. (1985). Further analysis of the Joyner-Boore attenuation data, Bull. Seismol. Soc. Am., 75(2): 611–614.

Campbell K.W., Bozorgnia Y. (2007). Campbell-Bozorgnia NGA ground motion relations for the geometric mean horizontal component of peak and spectral ground motion parameters, Tech. Rept. No. 2007/02, Pacific Earthquake Engineering Research Center, Berkeley, CA. 238 pgs.

Campbell K.W., Bozorgnia Y. (2008). NGA ground motion model for the geometric mean horizontal component of PGA, PGV, PGD and 5% damped linear elastic response spectra for periods ranging from 0.01 to 10 s, Earthq. Spectra 24(1): 139–171.

Chiou B., Darragh R., Gregor N., Silva W.J. (2008). NGA project strong-motion database, Earthq. Spectra, 24 (1): 23–44.

HastieT., Tibshirani R., Friedman J.H. (2001). The Elements of Statistical Learning: Data Mining, Inference, and Prediction, New York: Springer-Verlag.

Huang Y., Whittaker A.S., Luco N. (2008). Maximum spectral demands in the near-fault region, Earthq. Spectra 24(1): 319–341.

Huang Y., Whittaker A.S., Luco N. (2011). Establishing maximum spectral demand for performance-based earthquake engineering: collaborative research with the University at Buffalo and the USGS, USGS Technical Report: Award Number 08HQGR0017, United States Geological Survey, Reston, VA.

Jayaram N., Baker J.W. (2008). Statistical tests of the joint distribution of spectral acceleration values, Bull. Seismol. Soc. Am., 98(5): 2231–2243.

NEHRP (2009). NEHRP Recommended Provisions for Seismic Regulations for New Buildings and Other Structures, FEMA P-750. Federal Emergency Management Agency, Washington D.C.

Searle S. (1971). Linear Models, John Wiley and Sons, Inc., New York, 560 pgs.

Somerville P.G., Smith N.F., Graves R.W., Abrahamson N.A. (1997). Modification of empirical strong ground-motion attenuation relations to include the amplitude and duration effects of rupture directivity, Seismol. Res. Lett.,68(1): 199–222.

Spudich P., Watson-Lamprey J., Somerville P., Bayless J., Shahi S.K., Baker J.W., Rowshandel B., Chiou B. (2012). Directivity models produced for the Next Generation Attenuation West 2 (NGA-West 2) project, Proceedings, 15th World Conference on Earthquake Engineering, Lisbon, Portugal.

Stewart J.P., Abrahamson N.A, Atkinson G.M., Baker J.W., Boore D.M., Bozorgnia Y., Campbell K.W., Comartin C.D., Idriss I.M., Lew M., Mehrain M., Moehle J.P., Naeim F., Sabol T.A. (2011). Representation of bi-directional ground motions for design spectra in building codes, Earthq. Spectra, 27(3): 927–937.

Watson-Lamprey J., Boore D.M. (2007). Beyond SaGMRotI: conversion to SaArb, SaSN, and SaMaxRot, Bull. Seismol. Soc. Am., 97(5): 1511–1524.

Appendix A: Dependence of $Sa_{RotD100}/Sa_{RotD50}$ on Seismological Parameters

This appendix contains figures showing the dependence of $Sa_{RotD100}/Sa_{RotD50}$ ratio on several seismological parameters. Each figure shows the scatter plot of $Sa_{RotD100}/Sa_{RotD50}$ ratios computed using a subset of NGA-West2 database being used to develop the Abrahamson-Silva ground-motion model. Median $Sa_{RotD100}/Sa_{RotD50}$ ratios from Table 3.1, and a non-parametric moving average model computed using LOESS smoothing (e.g., Hastie et al. [2001]) are also shown.

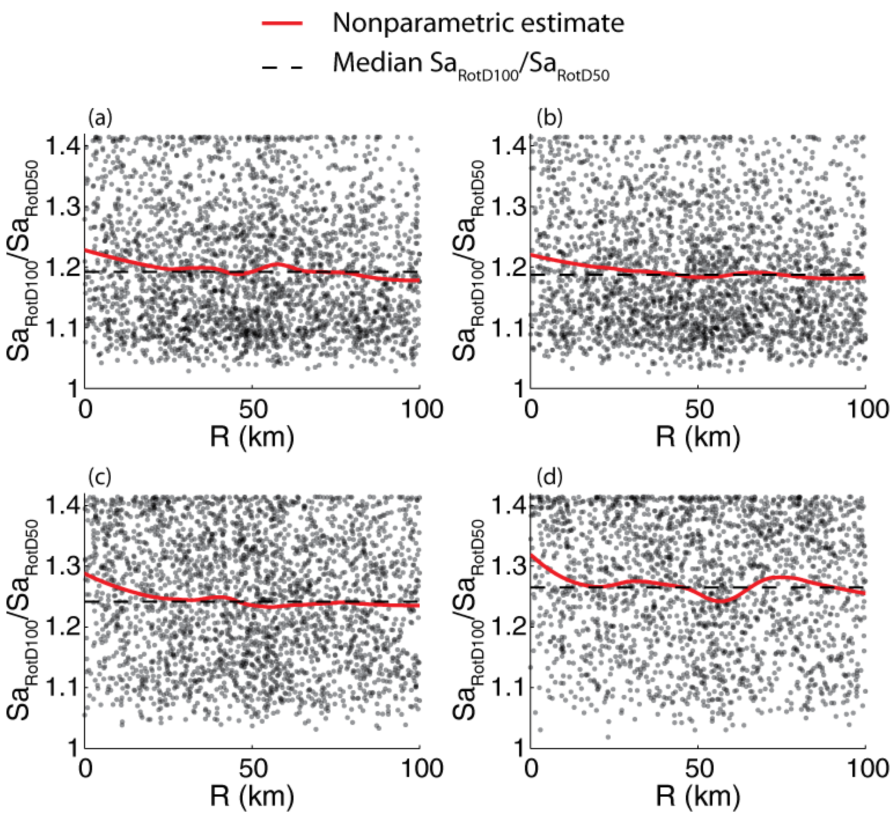

Figure A.1 **Dependence of $Sa_{RotD100}/Sa_{RotD50}$ on closest distance between site and the rupture surface (R). Figures are shown for spectral acceleration periods of (a) 0.01 sec, (b) 0.1 sec, (c) 1 sec, and (d) 5 sec. The median $Sa_{RotD100}/Sa_{RotD50}$ ratios are taken from Table 3.1, and the nonparametric estimate is computed using LOESS smoothing (e.g., Hastie et al., 2001).**

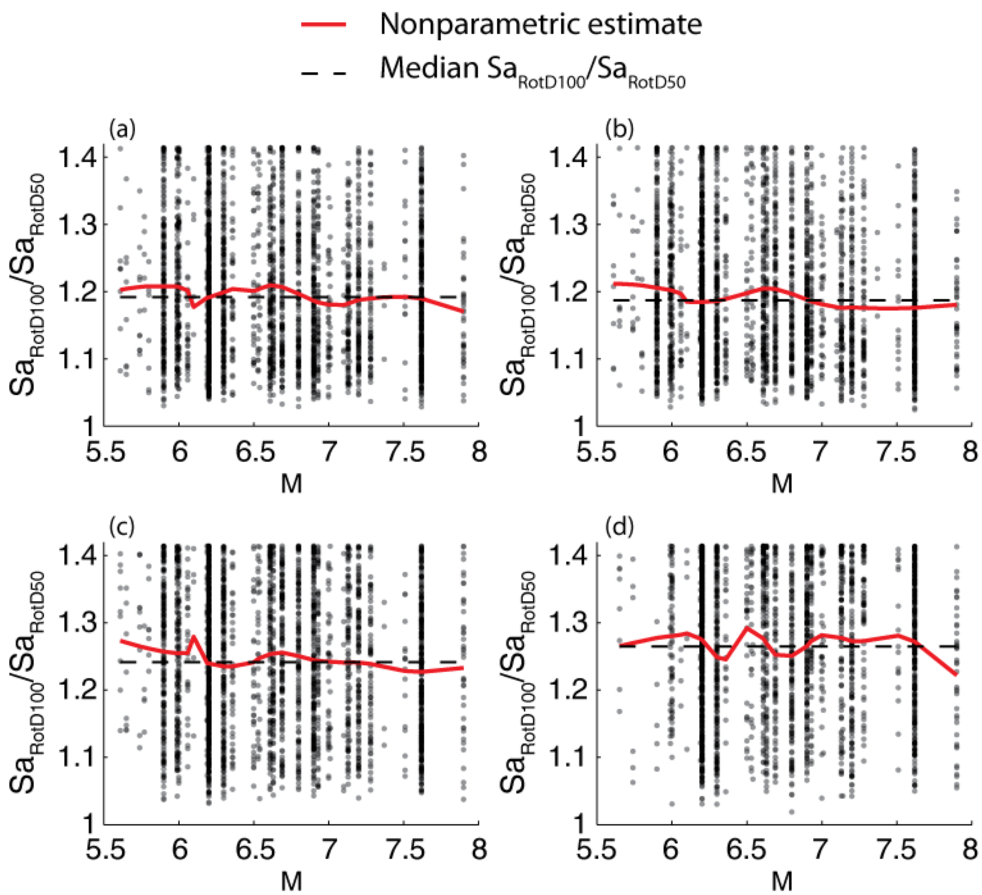

Figure A.2 **Dependence of $Sa_{RotD100}/Sa_{RotD50}$ on earthquake magnitude (M). Figures are shown for spectral acceleration periods of (a) 0.01 sec, (b) 0.1 sec, (c) 1 sec, and (d) 5 sec. The median $Sa_{RotD100}/Sa_{RotD50}$ ratios are taken from Table 3.1, and the nonparametric estimate is computed using LOESS smoothing (e.g., Hastie et al. [2001]).**

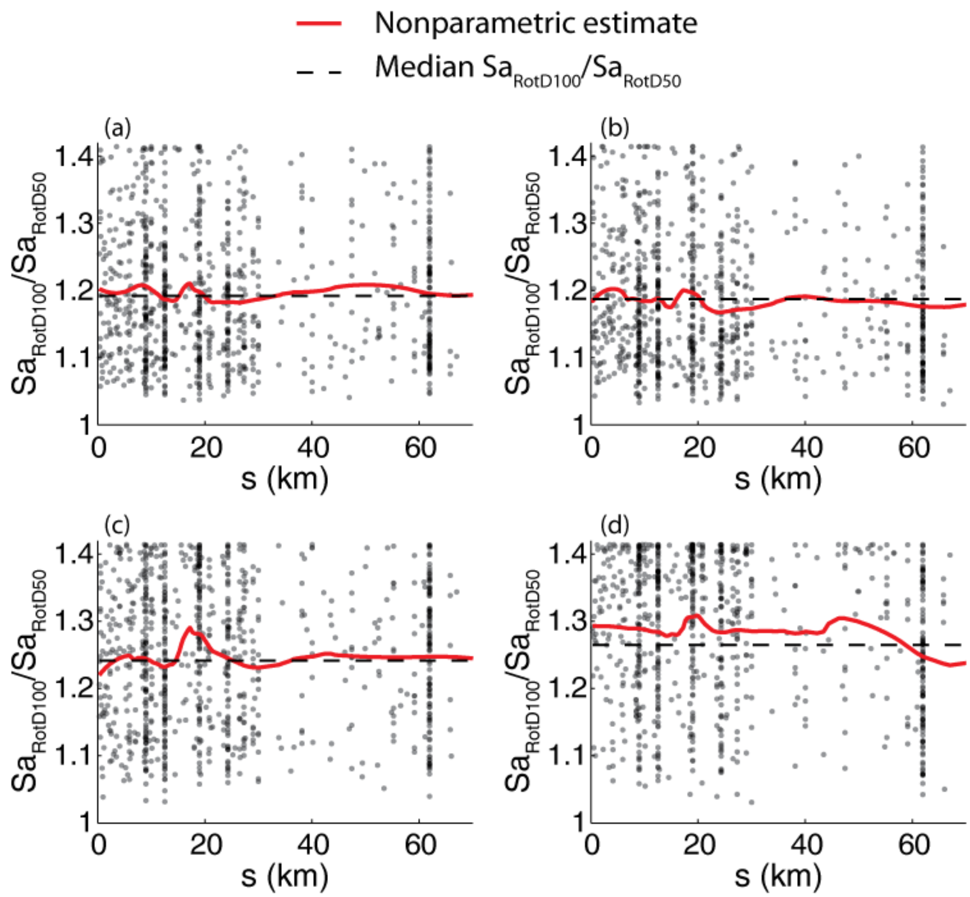

Figure A.3 **Dependence of $Sa_{RotD100}/Sa_{RotD50}$ on s, the length of rupture between the epicenter and the point on fault closest to the site [Somerville et al 1997], for strike-slip faults. Figures are shown for spectral acceleration periods of (a) 0.01 sec, (b) 0.1 sec, (c) 1 sec, and (d) 5 sec. The median $Sa_{RotD100}/Sa_{RotD50}$ ratios are taken from Table 3.1 and the nonparametric estimate is computed using LOESS smoothing (e.g., Hastie et al. [2001]).**

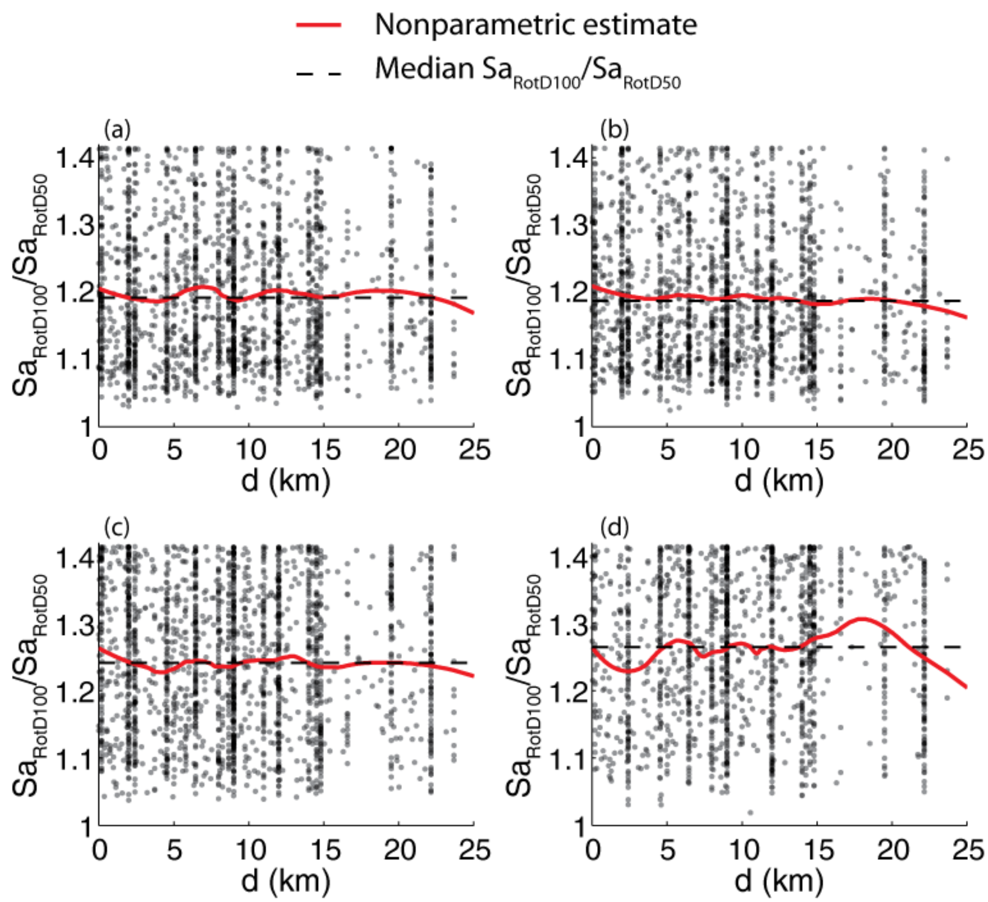

Figure A.4 **Dependence of $Sa_{RotD100}/Sa_{RotD50}$ on *d*, the length of rupture between the hypocenter and the point on fault closest to the site [Somerville et al. 1997], for non-strike-slip faults. Figures are shown for spectral acceleration periods of (a) 0.01 sec, (b) 0.1 sec, (c) 1 sec, and (d) 5 sec. The median $Sa_{RotD100}/Sa_{RotD50}$ ratios are taken from Table 3.1, and the nonparametric estimate is computed using LOESS smoothing (e.g., Hastie et al. [2001]).**

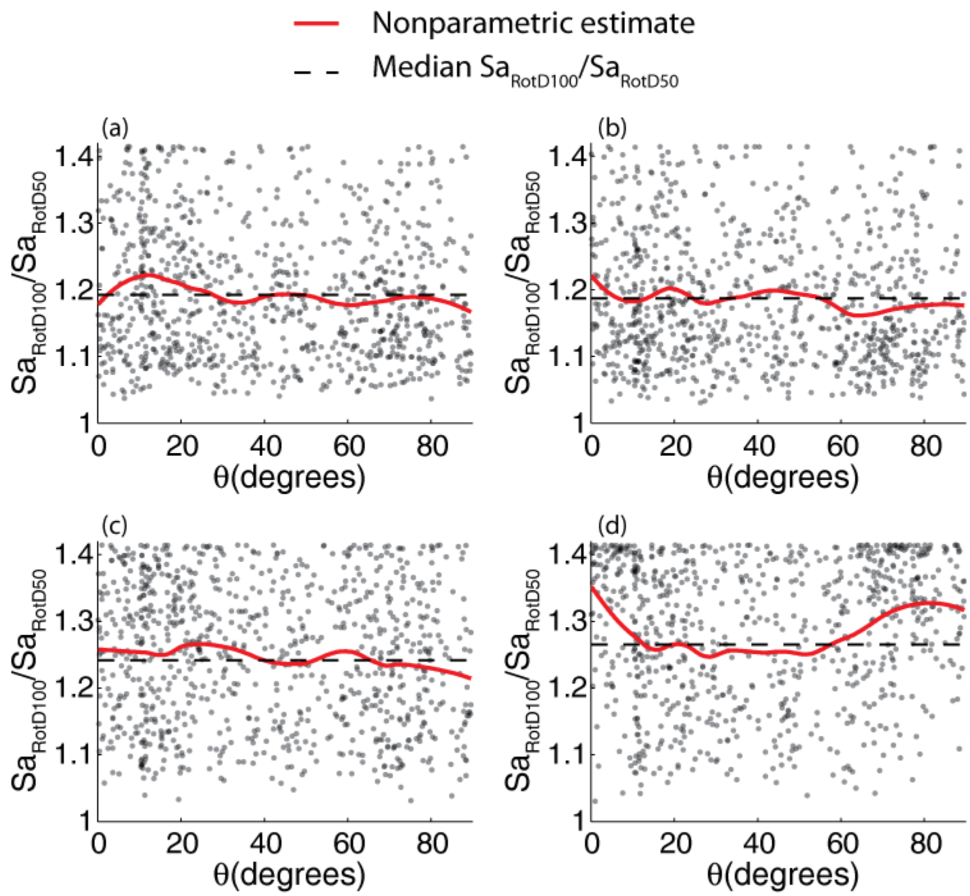

Figure A.5 **Dependence of $Sa_{RotD100}/Sa_{RotD50}$ on θ, the angle between the line joining the epicenter with the site and the strike of the fault [Somerville et al., 1997], for strike-slip fault. Figures are shown for spectral acceleration periods of (a) 0.01 sec, (b) 0.1 sec, (c) 1 sec, and (d) 5 sec. The median $Sa_{RotD100}/Sa_{RotD50}$ ratios are taken from Table 3.1, and the nonparametric estimate is computed using LOESS smoothing (e.g., Hastie et al. [2001]).**

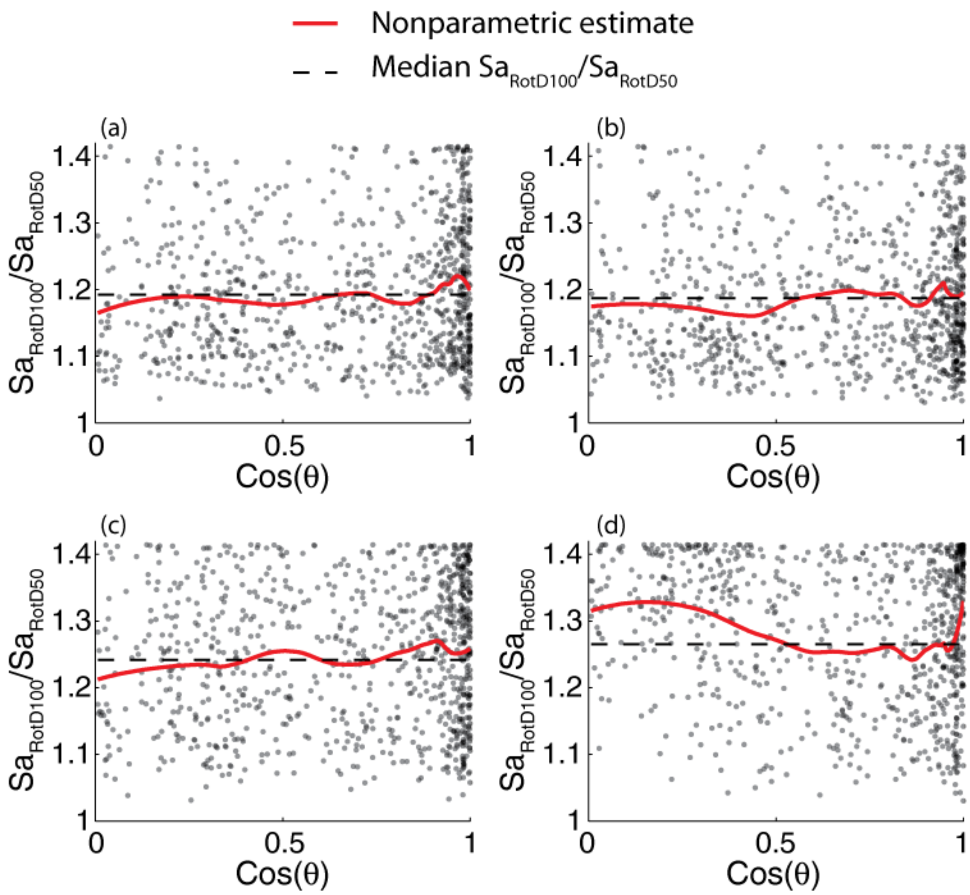

Figure A.6 **Dependence of $Sa_{RotD100}/Sa_{RotD50}$ on $\cos(\theta)$ for strike-slip faults. Figures are shown for spectral acceleration periods of (a) 0.01 sec, (b) 0.1 sec, (c) 1 sec, and (d) 5 sec. The median $Sa_{RotD100}/Sa_{RotD50}$ ratios are taken from Table 3.1, and the nonparametric estimate is computed using LOESS smoothing (e.g., Hastie et al., 2001).**

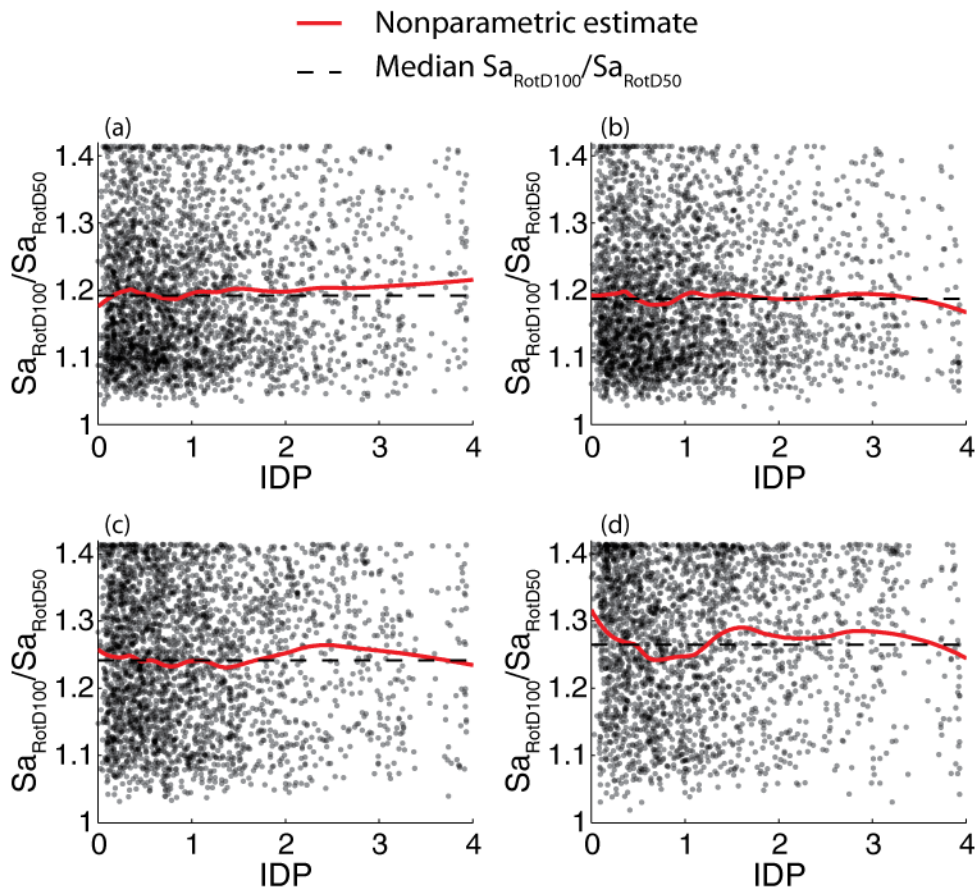

Figure A.7 **Dependence of $Sa_{RotD100}/Sa_{RotD50}$ on Spudich and Chiou's directivity parameter, IDP [Spudich et al. 2012]. Figures are shown for spectral acceleration periods of (a) 0.01 sec, (b) 0.1 sec, (c) 1 sec, and (d) 5 sec. The median $Sa_{RotD100}/Sa_{RotD50}$ ratios are taken from Table 3.1, and the nonparametric estimate is computed using LOESS smoothing (e.g., Hastie et al. [2001]).**

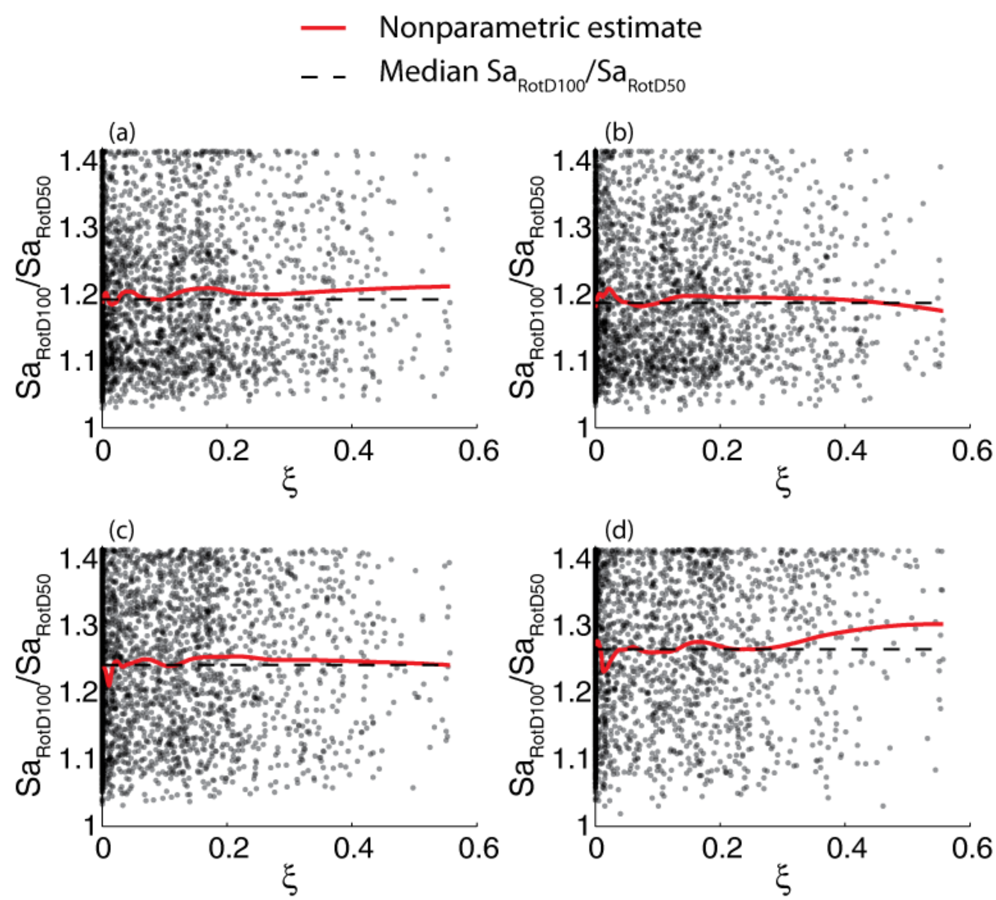

Figure A.8 **Dependence of $Sa_{RotD100}/Sa_{RotD50}$ on Rowshandel's directivity parameter, ξ [Spudich et al. 2012]. Figures are shown for spectral acceleration periods of (a) 0.01 sec, (b) 0.1 sec, (c) 1 sec, and (d) 5 sec. The median $Sa_{RotD100}/Sa_{RotD50}$ ratios are taken from Table 3.1, and the nonparametric estimate is computed using LOESS smoothing (e.g., Hastie et al. [2001]).**

Appendix B: Dependence of $Sa_{RotD100}$ Orientation on Directivity Parameters

This appendix contains figures showing histograms of the orientations with respect to the strike of the fault (α) in which $Sa_{RotD100}$ was observed. The histograms are binned into different distance and directivity parameter bins.

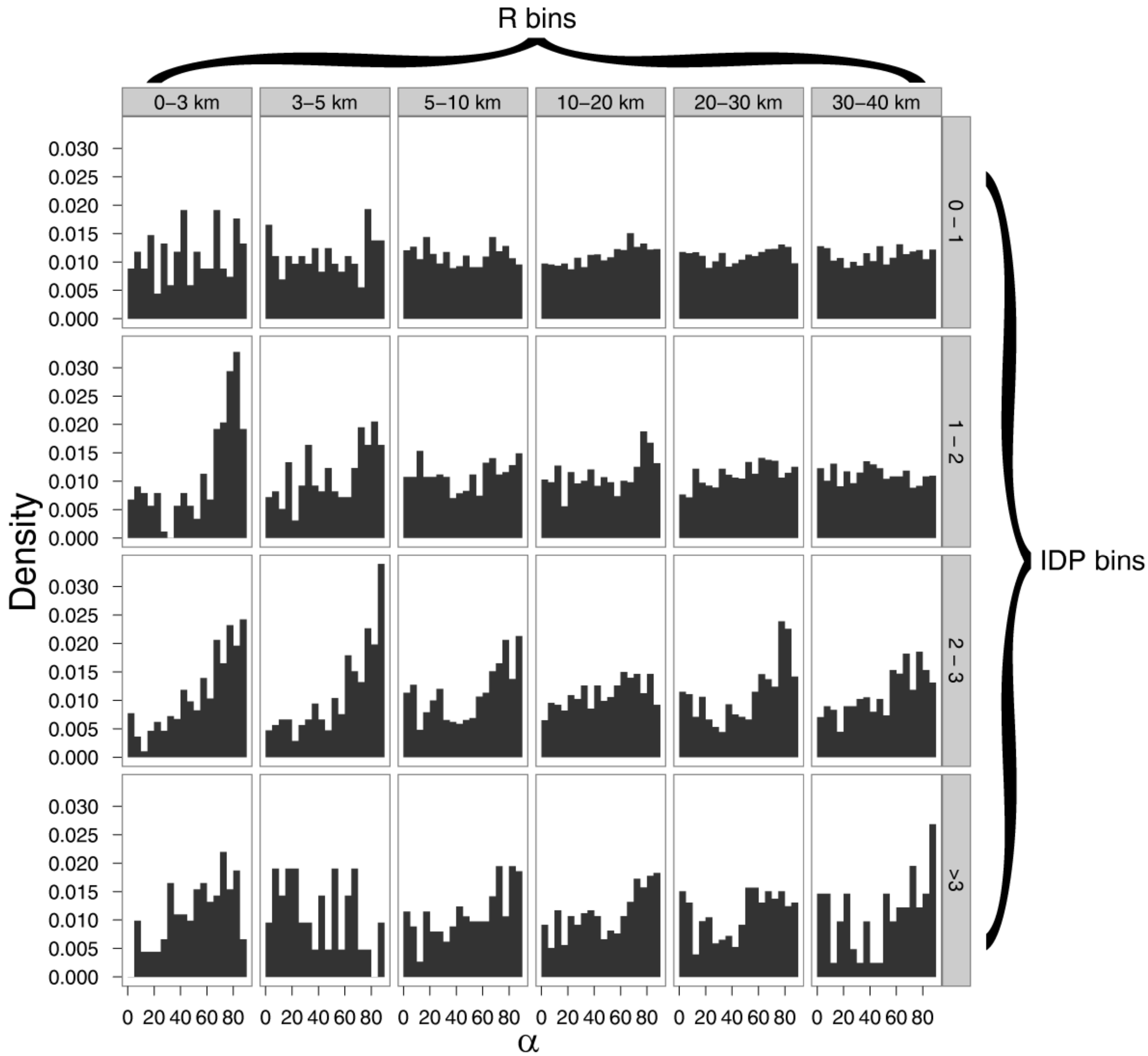

Figure B.1 **Probability density of α ($Sa_{RotD100}$ orientations) in different *R*, and Spudich and Chiou's directivity parameter (IDP) bins. The distance between site and fault rupture (*R*) is the primary factor affecting α, among the two factors considered here.**

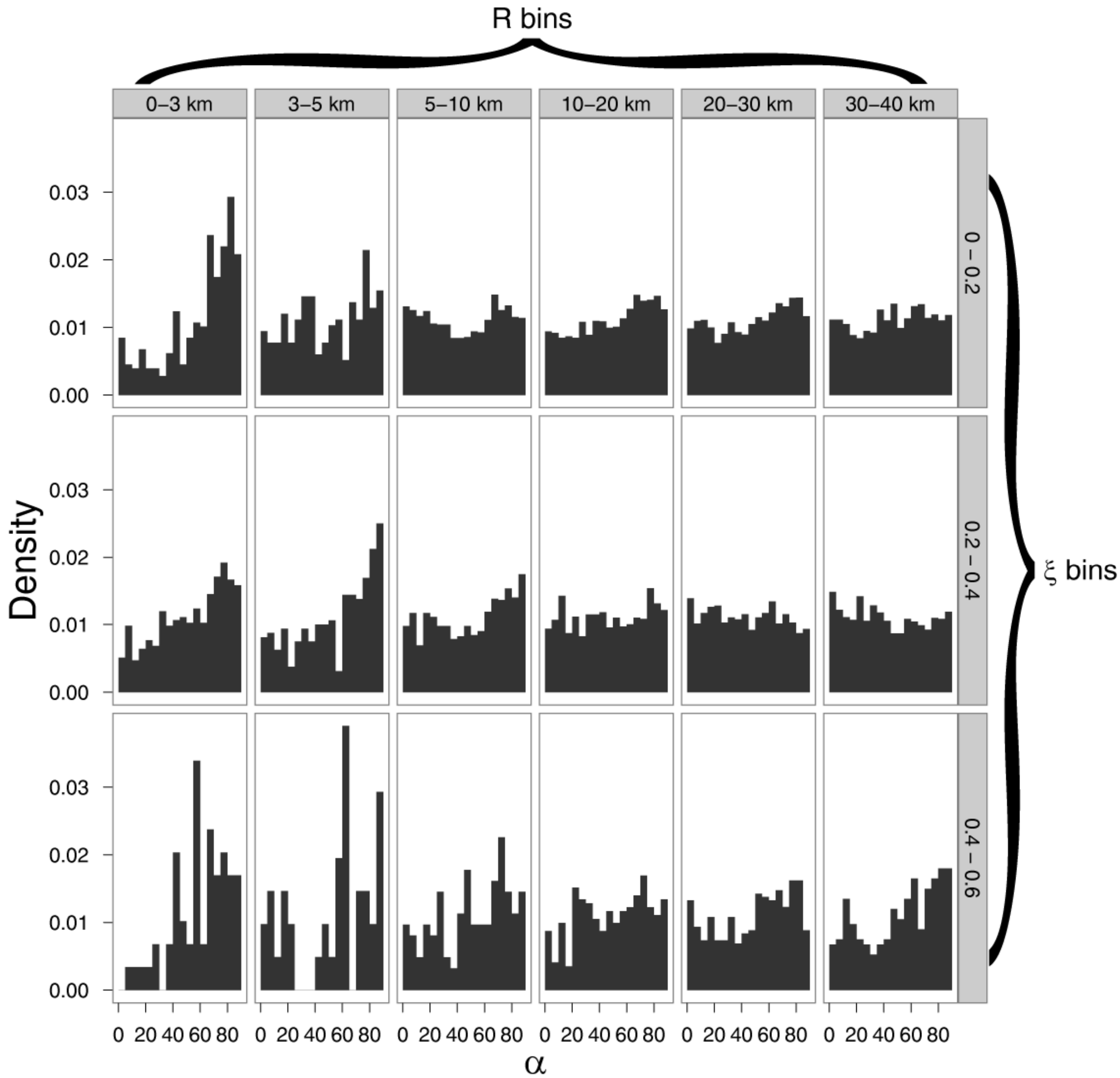

Figure B.2 **Probability density of α ($Sa_{RotD100}$ orientations) in different *R*, and Rowshandel's directivity parameter (ξ) bins. The distance between site and fault rupture (*R*) is the primary factor affecting α, among the two factors considered here.**

PEER REPORTS

PEER reports are available as a free PDF download from http://peer.berkeley.edu/publications/peer_reports_complete.html. Printed hard copies of PEER reports can be ordered directly from our printer by following the instructions at http://peer.berkeley.edu/publications/peer_reports.html. For other related questions about the PEER Report Series, contact the Pacific Earthquake Engineering Research Center, 325 Davis Hall mail code 1792, Berkeley, CA 94720. Tel.: (510) 642-3437; Fax: (510) 665-1655; Email: peer_editor@berkeley.edu

PEER 2013/10 *NGA-West2 Models for Ground-Motion Directionality.* Shrey K. Shahi and Jack W. Baker. May 2013.

PEER 2013/09 *Final Report of the NGA-West2 Directivity Working Group.* Paul Spudich, Jeffrey R. Bayless, Jack W. Baker, Brian S.J. Chiou, Badie Rowshandel, Shrey K. Shahi, and Paul Somerville. May 2013.

PEER 2013/08 *NGA-West2 Model for Estimating Average Horizontal Values of Pseudo-Absolute Spectral Accelerations Generated by Crustal Earthquakes.* I. M. Idriss. May 2013.

PEER 2013/07 *Update of the Chiou and Youngs NGA Ground Motion Model for Average Horizontal Component of Peak Ground Motion and Response Spectra.* Brian S.J. Chiou and Robert R. Youngs. May 2013.

PEER 2013/06 *NGA-West2 Campbell-Bozorgnia Ground Motion Model for the Horizontal Components of PGA, PGV, and 5%-Damped Elastic Pseudo-Acceleration Response Spectra for Periods Ranging from 0.01 to 10 sec.* Kenneth W. Campbell and Yousef Bozorgnia. May 2013.

PEER 2013/05 *NGA-West2 Equations for Predicting Response Spectral Accelerations for Shallow Crustal Earthquakes.* David M. Boore, Jonathan P. Stewart, Emel Seyhan, Gail M. Atkinson. May 2013.

PEER 2013/04 *Update of the AS08 Ground-Motion Prediction Equations Based on the NGA-West2 Data Set.* Norman SA. Abrahamson, Walter J. Silva, and Ronnie Kamai. May 2013.

PEER 2013/03 *PEER NGA-West2 Database.* Timothy D. Ancheta, Robert B. Darragh, Jonathan P. Stewart, Emel Seyhan, Walter J. Silva, Brian S.J. Chiou, Katie E. Wooddell, Robert W. Graves, Albert R. Kottke, David M. Boore, Tadahiro Kishida, and Jennifer L. Donahue. May 2013.

PEER 2013/02 *Hybrid Simulation of the Seismic Response of Squat Reinforced Concrete Shear Walls.* Catherine A. Whyte and Bozidar Stojadinovic. May 2013.

PEER 2013/01 *Housing Recovery in Chile: A Qualitative Mid-program Review.* Mary C. Comerio. February 2013.

PEER 2012/08 *Guidelines for Estimation of Shear Wave Velocity.* Bernard R. Wair, Jason T. DeJong, and Thomas Shantz. December 2012.

PEER 2012/07 *Earthquake Engineering for Resilient Communities: 2012 PEER Internship Program Research Report Collection.* Heidi Tremayne (Editor), Stephen A. Mahin (Editor), Collin Anderson, Dustin Cook, Michael Erceg, Carlos Esparza, Jose Jimenez, Dorian Krausz, Andrew Lo, Stephanie Lopez, Nicole McCurdy, Paul Shipman, Alexander Strum, Eduardo Vega. December 2012.

PEER 2012/06 *Fragilities for Precarious Rocks at Yucca Mountain.* Matthew D. Purvance, Rasool Anooshehpoor, and James N. Brune. December 2012.

PEER 2012/05 *Development of Simplified Analysis Procedure for Piles in Laterally Spreading Layered Soils.* Christopher R. McGann, Pedro Arduino, and Peter Mackenzie–Helnwein. December 2012.

PEER 2012/04 *Unbonded Pre-Tensioned Columns for Bridges in Seismic Regions.* Phillip M. Davis, Todd M. Janes, Marc O. Eberhard, and John F. Stanton. December 2012.

PEER 2012/03 *Experimental and Analytical Studies on Reinforced Concrete Buildings with Seismically Vulnerable Beam-Column Joints.* Sangjoon Park and Khalid M. Mosalam. October 2012.

PEER 2012/02 *Seismic Performance of Reinforced Concrete Bridges Allowed to Uplift during Multi-Directional Excitation.* Andres Oscar Espinoza and Stephen A. Mahin. July 2012.

PEER 2012/01 *Spectral Damping Scaling Factors for Shallow Crustal Earthquakes in Active Tectonic Regions.* Sanaz Rezaeian, Yousef Bozorgnia, I. M. Idriss, Kenneth Campbell, Norman Abrahamson, and Walter Silva. July 2012.

PEER 2011/10 *Earthquake Engineering for Resilient Communities: 2011 PEER Internship Program Research Report Collection.* Eds. Heidi Faison and Stephen A. Mahin. December 2011.

PEER 2011/09 *Calibration of Semi-Stochastic Procedure for Simulating High-Frequency Ground Motions.* Jonathan P. Stewart, Emel Seyhan, and Robert W. Graves. December 2011.

PEER 2011/08 *Water Supply in regard to Fire Following Earthquake.* Charles Scawthorn. November 2011.

PEER 2011/07 *Seismic Risk Management in Urban Areas. Proceedings of a U.S.-Iran-Turkey Seismic Workshop.* September 2011.

PEER 2011/06 *The Use of Base Isolation Systems to Achieve Complex Seismic Performance Objectives.* Troy A. Morgan and Stephen A. Mahin. July 2011.

PEER 2011/05 *Case Studies of the Seismic Performance of Tall Buildings Designed by Alternative Means.* Task 12 Report for the Tall Buildings Initiative. Jack Moehle, Yousef Bozorgnia, Nirmal Jayaram, Pierson Jones, Mohsen Rahnama, Nilesh Shome, Zeynep Tuna, John Wallace, Tony Yang, and Farzin Zareian. July 2011.

PEER 2011/04 *Recommended Design Practice for Pile Foundations in Laterally Spreading Ground.* Scott A. Ashford, Ross W. Boulanger, and Scott J. Brandenberg. June 2011.

PEER 2011/03 *New Ground Motion Selection Procedures and Selected Motions for the PEER Transportation Research Program.* Jack W. Baker, Ting Lin, Shrey K. Shahi, and Nirmal Jayaram. March 2011.

PEER 2011/02 *A Bayesian Network Methodology for Infrastructure Seismic Risk Assessment and Decision Support.* Michelle T. Bensi, Armen Der Kiureghian, and Daniel Straub. March 2011.

PEER 2011/01 *Demand Fragility Surfaces for Bridges in Liquefied and Laterally Spreading Ground.* Scott J. Brandenberg, Jian Zhang, Pirooz Kashighandi, Yili Huo, and Minxing Zhao. March 2011.

PEER 2010/05 *Guidelines for Performance-Based Seismic Design of Tall Buildings.* Developed by the Tall Buildings Initiative. November 2010.

PEER 2010/04 *Application Guide for the Design of Flexible and Rigid Bus Connections between Substation Equipment Subjected to Earthquakes.* Jean-Bernard Dastous and Armen Der Kiureghian. September 2010.

PEER 2010/03 *Shear Wave Velocity as a Statistical Function of Standard Penetration Test Resistance and Vertical Effective Stress at Caltrans Bridge Sites.* Scott J. Brandenberg, Naresh Bellana, and Thomas Shantz. June 2010.

PEER 2010/02 *Stochastic Modeling and Simulation of Ground Motions for Performance-Based Earthquake Engineering.* Sanaz Rezaeian and Armen Der Kiureghian. June 2010.

PEER 2010/01 *Structural Response and Cost Characterization of Bridge Construction Using Seismic Performance Enhancement Strategies.* Ady Aviram, Božidar Stojadinović, Gustavo J. Parra-Montesinos, and Kevin R. Mackie. March 2010.

PEER 2009/03 *The Integration of Experimental and Simulation Data in the Study of Reinforced Concrete Bridge Systems Including Soil-Foundation-Structure Interaction.* Matthew Dryden and Gregory L. Fenves. November 2009.

PEER 2009/02 *Improving Earthquake Mitigation through Innovations and Applications in Seismic Science, Engineering, Communication, and Response. Proceedings of a U.S.-Iran Seismic Workshop.* October 2009.

PEER 2009/01 *Evaluation of Ground Motion Selection and Modification Methods: Predicting Median Interstory Drift Response of Buildings.* Curt B. Haselton, Ed. June 2009.

PEER 2008/10 *Technical Manual for Strata.* Albert R. Kottke and Ellen M. Rathje. February 2009.

PEER 2008/09 *NGA Model for Average Horizontal Component of Peak Ground Motion and Response Spectra.* Brian S.-J. Chiou and Robert R. Youngs. November 2008.

PEER 2008/08 *Toward Earthquake-Resistant Design of Concentrically Braced Steel Structures.* Patxi Uriz and Stephen A. Mahin. November 2008.

PEER 2008/07 *Using OpenSees for Performance-Based Evaluation of Bridges on Liquefiable Soils.* Stephen L. Kramer, Pedro Arduino, and HyungSuk Shin. November 2008.

PEER 2008/06 *Shaking Table Tests and Numerical Investigation of Self-Centering Reinforced Concrete Bridge Columns.* Hyung IL Jeong, Junichi Sakai, and Stephen A. Mahin. September 2008.

PEER 2008/05 *Performance-Based Earthquake Engineering Design Evaluation Procedure for Bridge Foundations Undergoing Liquefaction-Induced Lateral Ground Displacement.* Christian A. Ledezma and Jonathan D. Bray. August 2008.

PEER 2008/04 *Benchmarking of Nonlinear Geotechnical Ground Response Analysis Procedures.* Jonathan P. Stewart, Annie On-Lei Kwok, Yousseff M. A. Hashash, Neven Matasovic, Robert Pyke, Zhiliang Wang, and Zhaohui Yang. August 2008.

PEER 2008/03 *Guidelines for Nonlinear Analysis of Bridge Structures in California.* Ady Aviram, Kevin R. Mackie, and Božidar Stojadinović. August 2008.

PEER 2008/02 *Treatment of Uncertainties in Seismic-Risk Analysis of Transportation Systems.* Evangelos Stergiou and Anne S. Kiremidjian. July 2008.

PEER 2008/01 *Seismic Performance Objectives for Tall Buildings.* William T. Holmes, Charles Kircher, William Petak, and Nabih Youssef. August 2008.

PEER 2007/12 *An Assessment to Benchmark the Seismic Performance of a Code-Conforming Reinforced Concrete Moment-Frame Building.* Curt Haselton, Christine A. Goulet, Judith Mitrani-Reiser, James L. Beck, Gregory G. Deierlein, Keith A. Porter, Jonathan P. Stewart, and Ertugrul Taciroglu. August 2008.

PEER 2007/11 *Bar Buckling in Reinforced Concrete Bridge Columns.* Wayne A. Brown, Dawn E. Lehman, and John F. Stanton. February 2008.

PEER 2007/10 *Computational Modeling of Progressive Collapse in Reinforced Concrete Frame Structures.* Mohamed M. Talaat and Khalid M. Mosalam. May 2008.

PEER 2007/09 *Integrated Probabilistic Performance-Based Evaluation of Benchmark Reinforced Concrete Bridges.* Kevin R. Mackie, John-Michael Wong, and Božidar Stojadinović. January 2008.

PEER 2007/08 *Assessing Seismic Collapse Safety of Modern Reinforced Concrete Moment-Frame Buildings.* Curt B. Haselton and Gregory G. Deierlein. February 2008.

PEER 2007/07 *Performance Modeling Strategies for Modern Reinforced Concrete Bridge Columns.* Michael P. Berry and Marc O. Eberhard. April 2008.

PEER 2007/06 *Development of Improved Procedures for Seismic Design of Buried and Partially Buried Structures.* Linda Al Atik and Nicholas Sitar. June 2007.

PEER 2007/05 *Uncertainty and Correlation in Seismic Risk Assessment of Transportation Systems.* Renee G. Lee and Anne S. Kiremidjian. July 2007.

PEER 2007/04 *Numerical Models for Analysis and Performance-Based Design of Shallow Foundations Subjected to Seismic Loading.* Sivapalan Gajan, Tara C. Hutchinson, Bruce L. Kutter, Prishati Raychowdhury, José A. Ugalde, and Jonathan P. Stewart. May 2008.

PEER 2007/03 *Beam-Column Element Model Calibrated for Predicting Flexural Response Leading to Global Collapse of RC Frame Buildings.* Curt B. Haselton, Abbie B. Liel, Sarah Taylor Lange, and Gregory G. Deierlein. May 2008.

PEER 2007/02 *Campbell-Bozorgnia NGA Ground Motion Relations for the Geometric Mean Horizontal Component of Peak and Spectral Ground Motion Parameters.* Kenneth W. Campbell and Yousef Bozorgnia. May 2007.

PEER 2007/01 *Boore-Atkinson NGA Ground Motion Relations for the Geometric Mean Horizontal Component of Peak and Spectral Ground Motion Parameters.* David M. Boore and Gail M. Atkinson. May. May 2007.

PEER 2006/12 *Societal Implications of Performance-Based Earthquake Engineering.* Peter J. May. May 2007.

PEER 2006/11 *Probabilistic Seismic Demand Analysis Using Advanced Ground Motion Intensity Measures, Attenuation Relationships, and Near-Fault Effects.* Polsak Tothong and C. Allin Cornell. March 2007.

PEER 2006/10 *Application of the PEER PBEE Methodology to the I-880 Viaduct.* Sashi Kunnath. February 2007.

PEER 2006/09 *Quantifying Economic Losses from Travel Forgone Following a Large Metropolitan Earthquake.* James Moore, Sungbin Cho, Yue Yue Fan, and Stuart Werner. November 2006.

PEER 2006/08 *Vector-Valued Ground Motion Intensity Measures for Probabilistic Seismic Demand Analysis.* Jack W. Baker and C. Allin Cornell. October 2006.

PEER 2006/07 *Analytical Modeling of Reinforced Concrete Walls for Predicting Flexural and Coupled–Shear-Flexural Responses.* Kutay Orakcal, Leonardo M. Massone, and John W. Wallace. October 2006.

PEER 2006/06 *Nonlinear Analysis of a Soil-Drilled Pier System under Static and Dynamic Axial Loading.* Gang Wang and Nicholas Sitar. November 2006.

PEER 2006/05 *Advanced Seismic Assessment Guidelines.* Paolo Bazzurro, C. Allin Cornell, Charles Menun, Maziar Motahari, and Nicolas Luco. September 2006.

PEER 2006/04 *Probabilistic Seismic Evaluation of Reinforced Concrete Structural Components and Systems.* Tae Hyung Lee and Khalid M. Mosalam. August 2006.

PEER 2006/03 *Performance of Lifelines Subjected to Lateral Spreading.* Scott A. Ashford and Teerawut Juirnarongrit. July 2006.

PEER 2006/02 *Pacific Earthquake Engineering Research Center Highway Demonstration Project.* Anne Kiremidjian, James Moore, Yue Yue Fan, Nesrin Basoz, Ozgur Yazali, and Meredith Williams. April 2006.

PEER 2006/01 *Bracing Berkeley. A Guide to Seismic Safety on the UC Berkeley Campus.* Mary C. Comerio, Stephen Tobriner, and Ariane Fehrenkamp. January 2006.

PEER 2005/16 *Seismic Response and Reliability of Electrical Substation Equipment and Systems.* Junho Song, Armen Der Kiureghian, and Jerome L. Sackman. April 2006.

PEER 2005/15 *CPT-Based Probabilistic Assessment of Seismic Soil Liquefaction Initiation.* R. E. S. Moss, R. B. Seed, R. E. Kayen, J. P. Stewart, and A. Der Kiureghian. April 2006.

PEER 2005/14 *Workshop on Modeling of Nonlinear Cyclic Load-Deformation Behavior of Shallow Foundations.* Bruce L. Kutter, Geoffrey Martin, Tara Hutchinson, Chad Harden, Sivapalan Gajan, and Justin Phalen. March 2006.

PEER 2005/13 *Stochastic Characterization and Decision Bases under Time-Dependent Aftershock Risk in Performance-Based Earthquake Engineering.* Gee Liek Yeo and C. Allin Cornell. July 2005.

PEER 2005/12 *PEER Testbed Study on a Laboratory Building: Exercising Seismic Performance Assessment.* Mary C. Comerio, editor. November 2005.

PEER 2005/11 *Van Nuys Hotel Building Testbed Report: Exercising Seismic Performance Assessment.* Helmut Krawinkler, editor. October 2005.

PEER 2005/10 *First NEES/E-Defense Workshop on Collapse Simulation of Reinforced Concrete Building Structures.* September 2005.

PEER 2005/09 *Test Applications of Advanced Seismic Assessment Guidelines.* Joe Maffei, Karl Telleen, Danya Mohr, William Holmes, and Yuki Nakayama. August 2006.

PEER 2005/08 *Damage Accumulation in Lightly Confined Reinforced Concrete Bridge Columns.* R. Tyler Ranf, Jared M. Nelson, Zach Price, Marc O. Eberhard, and John F. Stanton. April 2006.

PEER 2005/07 *Experimental and Analytical Studies on the Seismic Response of Freestanding and Anchored Laboratory Equipment*. Dimitrios Konstantinidis and Nicos Makris. January 2005.

PEER 2005/06 *Global Collapse of Frame Structures under Seismic Excitations*. Luis F. Ibarra and Helmut Krawinkler. September 2005.

PEER 2005//05 *Performance Characterization of Bench- and Shelf-Mounted Equipment.* Samit Ray Chaudhuri and Tara C. Hutchinson. May 2006.

PEER 2005/04 *Numerical Modeling of the Nonlinear Cyclic Response of Shallow Foundations.* Chad Harden, Tara Hutchinson, Geoffrey R. Martin, and Bruce L. Kutter. August 2005.

PEER 2005/03 *A Taxonomy of Building Components for Performance-Based Earthquake Engineering.* Keith A. Porter. September 2005.

PEER 2005/02 *Fragility Basis for California Highway Overpass Bridge Seismic Decision Making*. Kevin R. Mackie and Božidar Stojadinović. June 2005.

PEER 2005/01 *Empirical Characterization of Site Conditions on Strong Ground Motion.* Jonathan P. Stewart, Yoojoong Choi, and Robert W. Graves. June 2005.

PEER 2004/09 *Electrical Substation Equipment Interaction: Experimental Rigid Conductor Studies.* Christopher Stearns and André Filiatrault. February 2005.

PEER 2004/08 *Seismic Qualification and Fragility Testing of Line Break 550-kV Disconnect Switches.* Shakhzod M. Takhirov, Gregory L. Fenves, and Eric Fujisaki. January 2005.

PEER 2004/07 *Ground Motions for Earthquake Simulator Qualification of Electrical Substation Equipment.* Shakhzod M. Takhirov, Gregory L. Fenves, Eric Fujisaki, and Don Clyde. January 2005.

PEER 2004/06 *Performance-Based Regulation and Regulatory Regimes.* Peter J. May and Chris Koski. September 2004.

PEER 2004/05 *Performance-Based Seismic Design Concepts and Implementation: Proceedings of an International Workshop.* Peter Fajfar and Helmut Krawinkler, editors. September 2004.

PEER 2004/04 *Seismic Performance of an Instrumented Tilt-up Wall Building.* James C. Anderson and Vitelmo V. Bertero. July 2004.

PEER 2004/03 *Evaluation and Application of Concrete Tilt-up Assessment Methodologies.* Timothy Graf and James O. Malley. October 2004.

PEER 2004/02 *Analytical Investigations of New Methods for Reducing Residual Displacements of Reinforced Concrete Bridge Columns.* Junichi Sakai and Stephen A. Mahin. August 2004.

PEER 2004/01 *Seismic Performance of Masonry Buildings and Design Implications.* Kerri Anne Taeko Tokoro, James C. Anderson, and Vitelmo V. Bertero. February 2004.

PEER 2003/18 *Performance Models for Flexural Damage in Reinforced Concrete Columns.* Michael Berry and Marc Eberhard. August 2003.

PEER 2003/17 *Predicting Earthquake Damage in Older Reinforced Concrete Beam-Column Joints.* Catherine Pagni and Laura Lowes. October 2004.

PEER 2003/16 *Seismic Demands for Performance-Based Design of Bridges.* Kevin Mackie and Božidar Stojadinović. August 2003.

PEER 2003/15 *Seismic Demands for Nondeteriorating Frame Structures and Their Dependence on Ground Motions.* Ricardo Antonio Medina and Helmut Krawinkler. May 2004.

PEER 2003/14 *Finite Element Reliability and Sensitivity Methods for Performance-Based Earthquake Engineering.* Terje Haukaas and Armen Der Kiureghian. April 2004.

PEER 2003/13 *Effects of Connection Hysteretic Degradation on the Seismic Behavior of Steel Moment-Resisting Frames.* Janise E. Rodgers and Stephen A. Mahin. March 2004.

PEER 2003/12 *Implementation Manual for the Seismic Protection of Laboratory Contents: Format and Case Studies.* William T. Holmes and Mary C. Comerio. October 2003.

PEER 2003/11 *Fifth U.S.-Japan Workshop on Performance-Based Earthquake Engineering Methodology for Reinforced Concrete Building Structures.* February 2004.

PEER 2003/10 *A Beam-Column Joint Model for Simulating the Earthquake Response of Reinforced Concrete Frames.* Laura N. Lowes, Nilanjan Mitra, and Arash Altoontash. February 2004.

PEER 2003/09 *Sequencing Repairs after an Earthquake: An Economic Approach.* Marco Casari and Simon J. Wilkie. April 2004.

PEER 2003/08 *A Technical Framework for Probability-Based Demand and Capacity Factor Design (DCFD) Seismic Formats.* Fatemeh Jalayer and C. Allin Cornell. November 2003.

PEER 2003/07 *Uncertainty Specification and Propagation for Loss Estimation Using FOSM Methods.* Jack W. Baker and C. Allin Cornell. September 2003.

PEER 2003/06 *Performance of Circular Reinforced Concrete Bridge Columns under Bidirectional Earthquake Loading*. Mahmoud M. Hachem, Stephen A. Mahin, and Jack P. Moehle. February 2003.

PEER 2003/05 *Response Assessment for Building-Specific Loss Estimation.* Eduardo Miranda and Shahram Taghavi. September 2003.

PEER 2003/04 *Experimental Assessment of Columns with Short Lap Splices Subjected to Cyclic Loads*. Murat Melek, John W. Wallace, and Joel Conte. April 2003.

PEER 2003/03 *Probabilistic Response Assessment for Building-Specific Loss Estimation.* Eduardo Miranda and Hesameddin Aslani. September 2003.

PEER 2003/02 *Software Framework for Collaborative Development of Nonlinear Dynamic Analysis Program.* Jun Peng and Kincho H. Law. September 2003.

PEER 2003/01 *Shake Table Tests and Analytical Studies on the Gravity Load Collapse of Reinforced Concrete Frames.* Kenneth John Elwood and Jack P. Moehle. November 2003.

PEER 2002/24 *Performance of Beam to Column Bridge Joints Subjected to a Large Velocity Pulse.* Natalie Gibson, André Filiatrault, and Scott A. Ashford. April 2002.

PEER 2002/23 *Effects of Large Velocity Pulses on Reinforced Concrete Bridge Columns.* Greg L. Orozco and Scott A. Ashford. April 2002.

PEER 2002/22 *Characterization of Large Velocity Pulses for Laboratory Testing.* Kenneth E. Cox and Scott A. Ashford. April 2002.

PEER 2002/21 *Fourth U.S.-Japan Workshop on Performance-Based Earthquake Engineering Methodology for Reinforced Concrete Building Structures*. December 2002.

PEER 2002/20 *Barriers to Adoption and Implementation of PBEE Innovations.* Peter J. May. August 2002.

PEER 2002/19 *Economic-Engineered Integrated Models for Earthquakes: Socioeconomic Impacts.* Peter Gordon, James E. Moore II, and Harry W. Richardson. July 2002.

PEER 2002/18 *Assessment of Reinforced Concrete Building Exterior Joints with Substandard Details.* Chris P. Pantelides, Jon Hansen, Justin Nadauld, and Lawrence D. Reaveley. May 2002.

PEER 2002/17 *Structural Characterization and Seismic Response Analysis of a Highway Overcrossing Equipped with Elastomeric Bearings and Fluid Dampers: A Case Study.* Nicos Makris and Jian Zhang. November 2002.

PEER 2002/16 *Estimation of Uncertainty in Geotechnical Properties for Performance-Based Earthquake Engineering.* Allen L. Jones, Steven L. Kramer, and Pedro Arduino. December 2002.

PEER 2002/15 *Seismic Behavior of Bridge Columns Subjected to Various Loading Patterns.* Asadollah Esmaeily-Gh. and Yan Xiao. December 2002.

PEER 2002/14 *Inelastic Seismic Response of Extended Pile Shaft Supported Bridge Structures.* T.C. Hutchinson, R.W. Boulanger, Y.H. Chai, and I.M. Idriss. December 2002.

PEER 2002/13 *Probabilistic Models and Fragility Estimates for Bridge Components and Systems.* Paolo Gardoni, Armen Der Kiureghian, and Khalid M. Mosalam. June 2002.

PEER 2002/12 *Effects of Fault Dip and Slip Rake on Near-Source Ground Motions: Why Chi-Chi Was a Relatively Mild M7.6 Earthquake.* Brad T. Aagaard, John F. Hall, and Thomas H. Heaton. December 2002.

PEER 2002/11 *Analytical and Experimental Study of Fiber-Reinforced Strip Isolators*. James M. Kelly and Shakhzod M. Takhirov. September 2002.

PEER 2002/10 *Centrifuge Modeling of Settlement and Lateral Spreading with Comparisons to Numerical Analyses***.** Sivapalan Gajan and Bruce L. Kutter. January 2003.

PEER 2002/09 *Documentation and Analysis of Field Case Histories of Seismic Compression during the 1994 Northridge, California, Earthquake.* Jonathan P. Stewart, Patrick M. Smith, Daniel H. Whang, and Jonathan D. Bray. October 2002.

PEER 2002/08 *Component Testing, Stability Analysis and Characterization of Buckling-Restrained Unbonded Braces™.* Cameron Black, Nicos Makris, and Ian Aiken. September 2002.

PEER 2002/07 *Seismic Performance of Pile-Wharf Connections.* Charles W. Roeder, Robert Graff, Jennifer Soderstrom, and Jun Han Yoo. December 2001.

PEER 2002/06 *The Use of Benefit-Cost Analysis for Evaluation of Performance-Based Earthquake Engineering Decisions*. Richard O. Zerbe and Anthony Falit-Baiamonte. September 2001.

PEER 2002/05 *Guidelines, Specifications, and Seismic Performance Characterization of Nonstructural Building Components and Equipment*. André Filiatrault, Constantin Christopoulos, and Christopher Stearns. September 2001.

PEER 2002/04 *Consortium of Organizations for Strong-Motion Observation Systems and the Pacific Earthquake Engineering Research Center Lifelines Program: Invited Workshop on Archiving and Web Dissemination of Geotechnical Data, 4–5 October 2001*. September 2002.

PEER 2002/03 *Investigation of Sensitivity of Building Loss Estimates to Major Uncertain Variables for the Van Nuys Testbed.* Keith A. Porter, James L. Beck, and Rustem V. Shaikhutdinov. August 2002.

PEER 2002/02 *The Third U.S.-Japan Workshop on Performance-Based Earthquake Engineering Methodology for Reinforced Concrete Building Structures*. July 2002.

PEER 2002/01 *Nonstructural Loss Estimation: The UC Berkeley Case Study.* Mary C. Comerio and John C. Stallmeyer. December 2001.

PEER 2001/16 *Statistics of SDF-System Estimate of Roof Displacement for Pushover Analysis of Buildings.* Anil K. Chopra, Rakesh K. Goel, and Chatpan Chintanapakdee. December 2001.

PEER 2001/15 *Damage to Bridges during the 2001 Nisqually Earthquake.* R. Tyler Ranf, Marc O. Eberhard, and Michael P. Berry. November 2001.

PEER 2001/14 *Rocking Response of Equipment Anchored to a Base Foundation.* Nicos Makris and Cameron J. Black. September 2001.

PEER 2001/13 *Modeling Soil Liquefaction Hazards for Performance-Based Earthquake Engineering.* Steven L. Kramer and Ahmed-W. Elgamal. February 2001.

PEER 2001/12 *Development of Geotechnical Capabilities in OpenSees.* Boris Jeremić. September 2001.

PEER 2001/11 *Analytical and Experimental Study of Fiber-Reinforced Elastomeric Isolators*. James M. Kelly and Shakhzod M. Takhirov. September 2001.

PEER 2001/10 *Amplification Factors for Spectral Acceleration in Active Regions.* Jonathan P. Stewart, Andrew H. Liu, Yoojoong Choi, and Mehmet B. Baturay. December 2001.

PEER 2001/09 *Ground Motion Evaluation Procedures for Performance-Based Design.* Jonathan P. Stewart, Shyh-Jeng Chiou, Jonathan D. Bray, Robert W. Graves, Paul G. Somerville, and Norman A. Abrahamson. September 2001.

PEER 2001/08 *Experimental and Computational Evaluation of Reinforced Concrete Bridge Beam-Column Connections for Seismic Performance.* Clay J. Naito, Jack P. Moehle, and Khalid M. Mosalam. November 2001.

PEER 2001/07 *The Rocking Spectrum and the Shortcomings of Design Guidelines.* Nicos Makris and Dimitrios Konstantinidis. August 2001.

PEER 2001/06 *Development of an Electrical Substation Equipment Performance Database for Evaluation of Equipment Fragilities*. Thalia Agnanos. April 1999.

PEER 2001/05 *Stiffness Analysis of Fiber-Reinforced Elastomeric Isolators.* Hsiang-Chuan Tsai and James M. Kelly. May 2001.

PEER 2001/04 *Organizational and Societal Considerations for Performance-Based Earthquake Engineering.* Peter J. May. April 2001.

PEER 2001/03 *A Modal Pushover Analysis Procedure to Estimate Seismic Demands for Buildings: Theory and Preliminary Evaluation.* Anil K. Chopra and Rakesh K. Goel. January 2001.

PEER 2001/02 *Seismic Response Analysis of Highway Overcrossings Including Soil-Structure Interaction.* Jian Zhang and Nicos Makris. March 2001.

PEER 2001/01 *Experimental Study of Large Seismic Steel Beam-to-Column Connections.* Egor P. Popov and Shakhzod M. Takhirov. November 2000.

PEER 2000/10 *The Second U.S.-Japan Workshop on Performance-Based Earthquake Engineering Methodology for Reinforced Concrete Building Structures.* March 2000.

PEER 2000/09 *Structural Engineering Reconnaissance of the August 17, 1999 Earthquake: Kocaeli (Izmit), Turkey.* Halil Sezen, Kenneth J. Elwood, Andrew S. Whittaker, Khalid Mosalam, John J. Wallace, and John F. Stanton. December 2000.

PEER 2000/08 *Behavior of Reinforced Concrete Bridge Columns Having Varying Aspect Ratios and Varying Lengths of Confinement.* Anthony J. Calderone, Dawn E. Lehman, and Jack P. Moehle. January 2001.

PEER 2000/07 *Cover-Plate and Flange-Plate Reinforced Steel Moment-Resisting Connections.* Taejin Kim, Andrew S. Whittaker, Amir S. Gilani, Vitelmo V. Bertero, and Shakhzod M. Takhirov. September 2000.

PEER 2000/06 *Seismic Evaluation and Analysis of 230-kV Disconnect Switches.* Amir S. J. Gilani, Andrew S. Whittaker, Gregory L. Fenves, Chun-Hao Chen, Henry Ho, and Eric Fujisaki. July 2000.

PEER 2000/05 *Performance-Based Evaluation of Exterior Reinforced Concrete Building Joints for Seismic Excitation.* Chandra Clyde, Chris P. Pantelides, and Lawrence D. Reaveley. July 2000.

PEER 2000/04 *An Evaluation of Seismic Energy Demand: An Attenuation Approach.* Chung-Che Chou and Chia-Ming Uang. July 1999.

PEER 2000/03 *Framing Earthquake Retrofitting Decisions: The Case of Hillside Homes in Los Angeles.* Detlof von Winterfeldt, Nels Roselund, and Alicia Kitsuse. March 2000.

PEER 2000/02 *U.S.-Japan Workshop on the Effects of Near-Field Earthquake Shaking.* Andrew Whittaker, ed. July 2000.

PEER 2000/01 *Further Studies on Seismic Interaction in Interconnected Electrical Substation Equipment.* Armen Der Kiureghian, Kee-Jeung Hong, and Jerome L. Sackman. November 1999.

PEER 1999/14 *Seismic Evaluation and Retrofit of 230-kV Porcelain Transformer Bushings.* Amir S. Gilani, Andrew S. Whittaker, Gregory L. Fenves, and Eric Fujisaki. December 1999.

PEER 1999/13 *Building Vulnerability Studies: Modeling and Evaluation of Tilt-up and Steel Reinforced Concrete Buildings.* John W. Wallace, Jonathan P. Stewart, and Andrew S. Whittaker, editors. December 1999.

PEER 1999/12 *Rehabilitation of Nonductile RC Frame Building Using Encasement Plates and Energy-Dissipating Devices.* Mehrdad Sasani, Vitelmo V. Bertero, James C. Anderson. December 1999.

PEER 1999/11 *Performance Evaluation Database for Concrete Bridge Components and Systems under Simulated Seismic Loads.* Yael D. Hose and Frieder Seible. November 1999.

PEER 1999/10 *U.S.-Japan Workshop on Performance-Based Earthquake Engineering Methodology for Reinforced Concrete Building Structures.* December 1999.

PEER 1999/09 *Performance Improvement of Long Period Building Structures Subjected to Severe Pulse-Type Ground Motions.* James C. Anderson, Vitelmo V. Bertero, and Raul Bertero. October 1999.

PEER 1999/08 *Envelopes for Seismic Response Vectors.* Charles Menun and Armen Der Kiureghian. July 1999.

PEER 1999/07 *Documentation of Strengths and Weaknesses of Current Computer Analysis Methods for Seismic Performance of Reinforced Concrete Members.* William F. Cofer. November 1999.

PEER 1999/06 *Rocking Response and Overturning of Anchored Equipment under Seismic Excitations.* Nicos Makris and Jian Zhang. November 1999.

PEER 1999/05 *Seismic Evaluation of 550 kV Porcelain Transformer Bushings.* Amir S. Gilani, Andrew S. Whittaker, Gregory L. Fenves, and Eric Fujisaki. October 1999.

PEER 1999/04 *Adoption and Enforcement of Earthquake Risk-Reduction Measures.* Peter J. May, Raymond J. Burby, T. Jens Feeley, and Robert Wood.

PEER 1999/03 *Task 3 Characterization of Site Response General Site Categories.* Adrian Rodriguez-Marek, Jonathan D. Bray, and Norman Abrahamson. February 1999.

PEER 1999/02 *Capacity-Demand-Diagram Methods for Estimating Seismic Deformation of Inelastic Structures: SDF Systems*. Anil K. Chopra and Rakesh Goel. April 1999.

PEER 1999/01 *Interaction in Interconnected Electrical Substation Equipment Subjected to Earthquake Ground Motions.* Armen Der Kiureghian, Jerome L. Sackman, and Kee-Jeung Hong. February 1999.

PEER 1998/08 *Behavior and Failure Analysis of a Multiple-Frame Highway Bridge in the 1994 Northridge Earthquake.* Gregory L. Fenves and Michael Ellery. December 1998.

PEER 1998/07 *Empirical Evaluation of Inertial Soil-Structure Interaction Effects.* Jonathan P. Stewart, Raymond B. Seed, and Gregory L. Fenves. November 1998.

PEER 1998/06 *Effect of Damping Mechanisms on the Response of Seismic Isolated Structures.* Nicos Makris and Shih-Po Chang. November 1998.

PEER 1998/05 *Rocking Response and Overturning of Equipment under Horizontal Pulse-Type Motions.* Nicos Makris and Yiannis Roussos. October 1998.

PEER 1998/04 *Pacific Earthquake Engineering Research Invitational Workshop Proceedings, May 14–15, 1998: Defining the Links between Planning, Policy Analysis, Economics and Earthquake Engineering.* Mary Comerio and Peter Gordon. September 1998.

PEER 1998/03 *Repair/Upgrade Procedures for Welded Beam to Column Connections.* James C. Anderson and Xiaojing Duan. May 1998.

PEER 1998/02 *Seismic Evaluation of 196 kV Porcelain Transformer Bushings.* Amir S. Gilani, Juan W. Chavez, Gregory L. Fenves, and Andrew S. Whittaker. May 1998.

PEER 1998/01 *Seismic Performance of Well-Confined Concrete Bridge Columns.* Dawn E. Lehman and Jack P. Moehle. December 2000.

ONLINE PEER REPORTS

The following PEER reports are available by Internet only at http://peer.berkeley.edu/publications/peer_reports_complete.html.

PEER 2012/103 *Performance-Based Seismic Demand Assessment of Concentrically Braced Steel Frame Buildings.* Chui-Hsin Chen and Stephen A. Mahin. December 2012.

PEER 2012/102 *Procedure to Restart an Interrupted Hybrid Simulation: Addendum to PEER Report 2010/103.* Vesna Terzic and Bozidar Stojadinovic. October 2012.

PEER 2012/101 *Mechanics of Fiber Reinforced Bearings.* James M. Kelly and Andrea Calabrese. February 2012.

PEER 2011/107 *Nonlinear Site Response and Seismic Compression at Vertical Array Strongly Shaken by 2007 Niigata-ken Chuetsu-oki Earthquake.* Eric Yee, Jonathan P. Stewart, and Kohji Tokimatsu. December 2011.

PEER 2011/106 *Self Compacting Hybrid Fiber Reinforced Concrete Composites for Bridge Columns.* Pardeep Kumar, Gabriel Jen, William Trono, Marios Panagiotou, and Claudia Ostertag. September 2011.

PEER 2011/105 *Stochastic Dynamic Analysis of Bridges Subjected to Spacially Varying Ground Motions.* Katerina Konakli and Armen Der Kiureghian. August 2011.

PEER 2011/104 *Design and Instrumentation of the 2010 E-Defense Four-Story Reinforced Concrete and Post-Tensioned Concrete Buildings.* Takuya Nagae, Kenichi Tahara, Taizo Matsumori, Hitoshi Shiohara, Toshimi Kabeyasawa, Susumu Kono, Minehiro Nishiyama (Japanese Research Team) and John Wallace, Wassim Ghannoum, Jack Moehle, Richard Sause, Wesley Keller, Zeynep Tuna (U.S. Research Team). June 2011.

PEER 2011/103 *In-Situ Monitoring of the Force Output of Fluid Dampers: Experimental Investigation.* Dimitrios Konstantinidis, James M. Kelly, and Nicos Makris. April 2011.

PEER 2011/102 *Ground-motion prediction equations 1964 - 2010.* John Douglas. April 2011.

PEER 2011/101 *Report of the Eighth Planning Meeting of NEES/E-Defense Collaborative Research on Earthquake Engineering.* Convened by the Hyogo Earthquake Engineering Research Center (NIED), NEES Consortium, Inc. February 2011.

PEER 2010/111 *Modeling and Acceptance Criteria for Seismic Design and Analysis of Tall Buildings.* Task 7 Report for the Tall Buildings Initiative - Published jointly by the Applied Technology Council. October 2010.

PEER 2010/110 *Seismic Performance Assessment and Probabilistic Repair Cost Analysis of Precast Concrete Cladding Systems for Multistory Buildlings.* Jeffrey P. Hunt and Božidar Stojadinovic. November 2010.

PEER 2010/109 *Report of the Seventh Joint Planning Meeting of NEES/E-Defense Collaboration on Earthquake Engineering. Held at the E-Defense, Miki, and Shin-Kobe, Japan, September 18–19, 2009.* August 2010.

PEER 2010/108 *Probabilistic Tsunami Hazard in California.* Hong Kie Thio, Paul Somerville, and Jascha Polet, preparers. October 2010.

PEER 2010/107 *Performance and Reliability of Exposed Column Base Plate Connections for Steel Moment-Resisting Frames.* Ady Aviram, Božidar Stojadinovic, and Armen Der Kiureghian. August 2010.

PEER 2010/106 *Verification of Probabilistic Seismic Hazard Analysis Computer Programs.* Patricia Thomas, Ivan Wong, and Norman Abrahamson. May 2010.

PEER 2010/105 *Structural Engineering Reconnaissance of the April 6, 2009, Abruzzo, Italy, Earthquake, and Lessons Learned.* M. Selim Günay and Khalid M. Mosalam. April 2010.

PEER 2010/104 *Simulating the Inelastic Seismic Behavior of Steel Braced Frames, Including the Effects of Low-Cycle Fatigue.* Yuli Huang and Stephen A. Mahin. April 2010.

PEER 2010/103 *Post-Earthquake Traffic Capacity of Modern Bridges in California.* Vesna Terzic and Božidar Stojadinović. March 2010.

PEER 2010/102 *Analysis of Cumulative Absolute Velocity (CAV) and JMA Instrumental Seismic Intensity (I_{JMA}) Using the PEER–NGA Strong Motion Database.* Kenneth W. Campbell and Yousef Bozorgnia. February 2010.

PEER 2010/101 *Rocking Response of Bridges on Shallow Foundations.* Jose A. Ugalde, Bruce L. Kutter, and Boris Jeremic. April 2010.

PEER 2009/109 *Simulation and Performance-Based Earthquake Engineering Assessment of Self-Centering Post-Tensioned Concrete Bridge Systems.* Won K. Lee and Sarah L. Billington. December 2009.

PEER 2009/108 *PEER Lifelines Geotechnical Virtual Data Center.* J. Carl Stepp, Daniel J. Ponti, Loren L. Turner, Jennifer N. Swift, Sean Devlin, Yang Zhu, Jean Benoit, and John Bobbitt. September 2009.

PEER 2009/107 *Experimental and Computational Evaluation of Current and Innovative In-Span Hinge Details in Reinforced Concrete Box-Girder Bridges: Part 2: Post-Test Analysis and Design Recommendations.* Matias A. Hube and Khalid M. Mosalam. December 2009.

PEER 2009/106 *Shear Strength Models of Exterior Beam-Column Joints without Transverse Reinforcement.* Sangjoon Park and Khalid M. Mosalam. November 2009.

PEER 2009/105 *Reduced Uncertainty of Ground Motion Prediction Equations through Bayesian Variance Analysis.* Robb Eric S. Moss. November 2009.

PEER 2009/104 *Advanced Implementation of Hybrid Simulation.* Andreas H. Schellenberg, Stephen A. Mahin, Gregory L. Fenves. November 2009.

PEER 2009/103 *Performance Evaluation of Innovative Steel Braced Frames.* T. Y. Yang, Jack P. Moehle, and Božidar Stojadinovic. August 2009.

PEER 2009/102 *Reinvestigation of Liquefaction and Nonliquefaction Case Histories from the 1976 Tangshan Earthquake.* Robb Eric Moss, Robert E. Kayen, Liyuan Tong, Songyu Liu, Guojun Cai, and Jiaer Wu. August 2009.

PEER 2009/101 *Report of the First Joint Planning Meeting for the Second Phase of NEES/E-Defense Collaborative Research on Earthquake Engineering.* Stephen A. Mahin et al. July 2009.

PEER 2008/104 *Experimental and Analytical Study of the Seismic Performance of Retaining Structures.* Linda Al Atik and Nicholas Sitar. January 2009.

PEER 2008/103 *Experimental and Computational Evaluation of Current and Innovative In-Span Hinge Details in Reinforced Concrete Box-Girder Bridges. Part 1: Experimental Findings and Pre-Test Analysis.* Matias A. Hube and Khalid M. Mosalam. January 2009.

PEER 2008/102 *Modeling of Unreinforced Masonry Infill Walls Considering In-Plane and Out-of-Plane Interaction.* Stephen Kadysiewski and Khalid M. Mosalam. January 2009.

PEER 2008/101 *Seismic Performance Objectives for Tall Buildings.* William T. Holmes, Charles Kircher, William Petak, and Nabih Youssef. August 2008.

PEER 2007/101 *Generalized Hybrid Simulation Framework for Structural Systems Subjected to Seismic Loading.* Tarek Elkhoraibi and Khalid M. Mosalam. July 2007.

PEER 2007/100 *Seismic Evaluation of Reinforced Concrete Buildings Including Effects of Masonry Infill Walls.* Alidad Hashemi and Khalid M. Mosalam. July 2007.

The Pacific Earthquake Engineering Research Center (PEER) is a multi-institutional research and education center with headquarters at the University of California, Berkeley. Investigators from over 20 universities, several consulting companies, and researchers at various state and federal government agencies contribute to research programs focused on performance-based earthquake engineering.

These research programs aim to identify and reduce the risks from major earthquakes to life safety and to the economy by including research in a wide variety of disciplines including structural and geotechnical engineering, geology/seismology, lifelines, transportation, architecture, economics, risk management, and public policy.

PEER is supported by federal, state, local, and regional agencies, together with industry partners.

PEER Core Institutions:
University of California, Berkeley (Lead Institution)
California Institute of Technology
Oregon State University
Stanford University
University of California, Davis
University of California, Irvine
University of California, Los Angeles
University of California, San Diego
University of Southern California
University of Washington

PEER reports can be ordered at http://peer.berkeley.edu/publications/peer_reports.html or by contacting

Pacific Earthquake Engineering Research Center
University of California, Berkeley
325 Davis Hall, mail code 1792
Berkeley, CA 94720-1792
Tel: 510-642-3437
Fax: 510-642-1655
Email: peer_editor@berkeley.edu

ISSN 1547-0587X